Table 4. Univariate and Multivariate Analyses of the Value of Each Variable in Predicting Cardiac Events

Predictive Factors During the Acute Phase	Univariate X^2	Univariate P	Multivariate X^2	Multivariate P
Age	3.13	0.076		
Reperfusion time	1.38	0.238		
Peak CK-MB	3.01	0.082		
Peak Tenascin-C	14.8	0.0001	10.82	0.001
BNP on day 5	4.32	0.037		
BNP on day 28	7.94	0.004	4.23	0.039
LVEDV	3.61	0.057		
LVESV	8.76	0.003	0.36	0.543
LVEF	6.96	0.008	0.76	0.381
Total Defect Scores	6.51	0.011	0.03	0.852

LVEDV = left ventricular end-diastolic volume; EF = ejection fraction

LVESV = left ventricular end-systolic volume

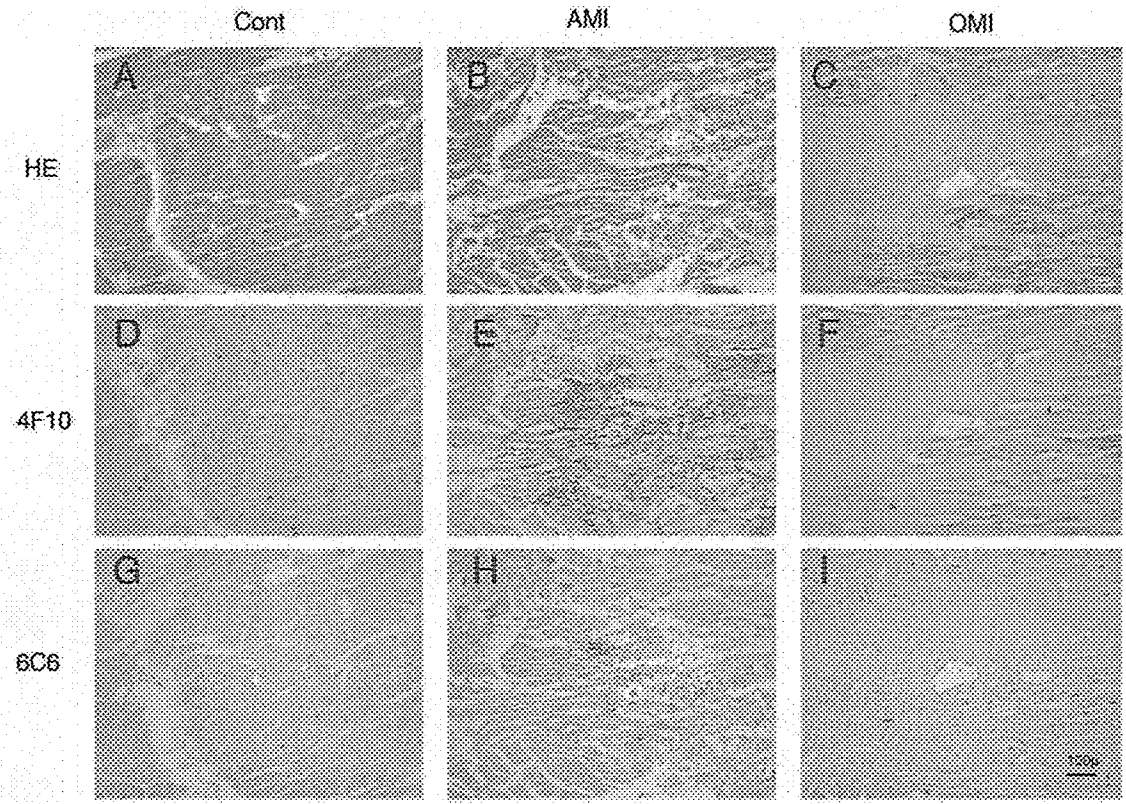
Cont
AMI
OMI
HE
4F10
6C6
A
B
C
D
E
F
G
H
I

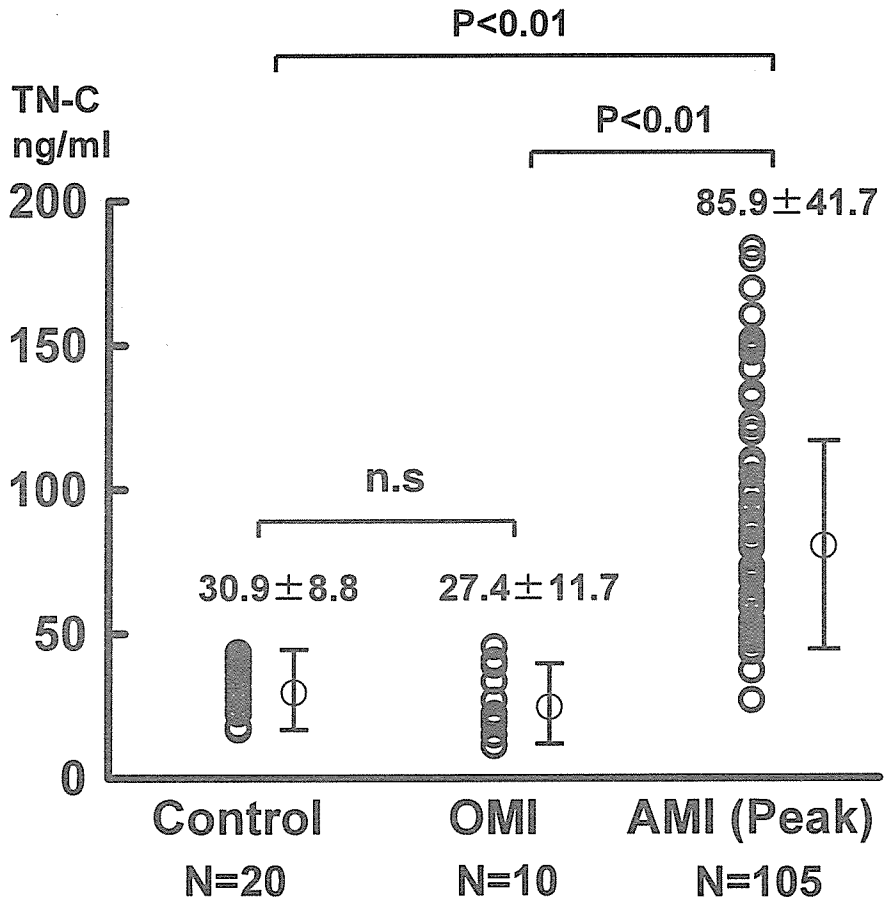
P<0.01
P<0.01
TN-C
ng/ml
200
150
100
50
0
85.9±41.7
n.s
30.9±8.8
27.4±11.7
Control
N=20
OMI
N=10
AMI (Peak)
N=105

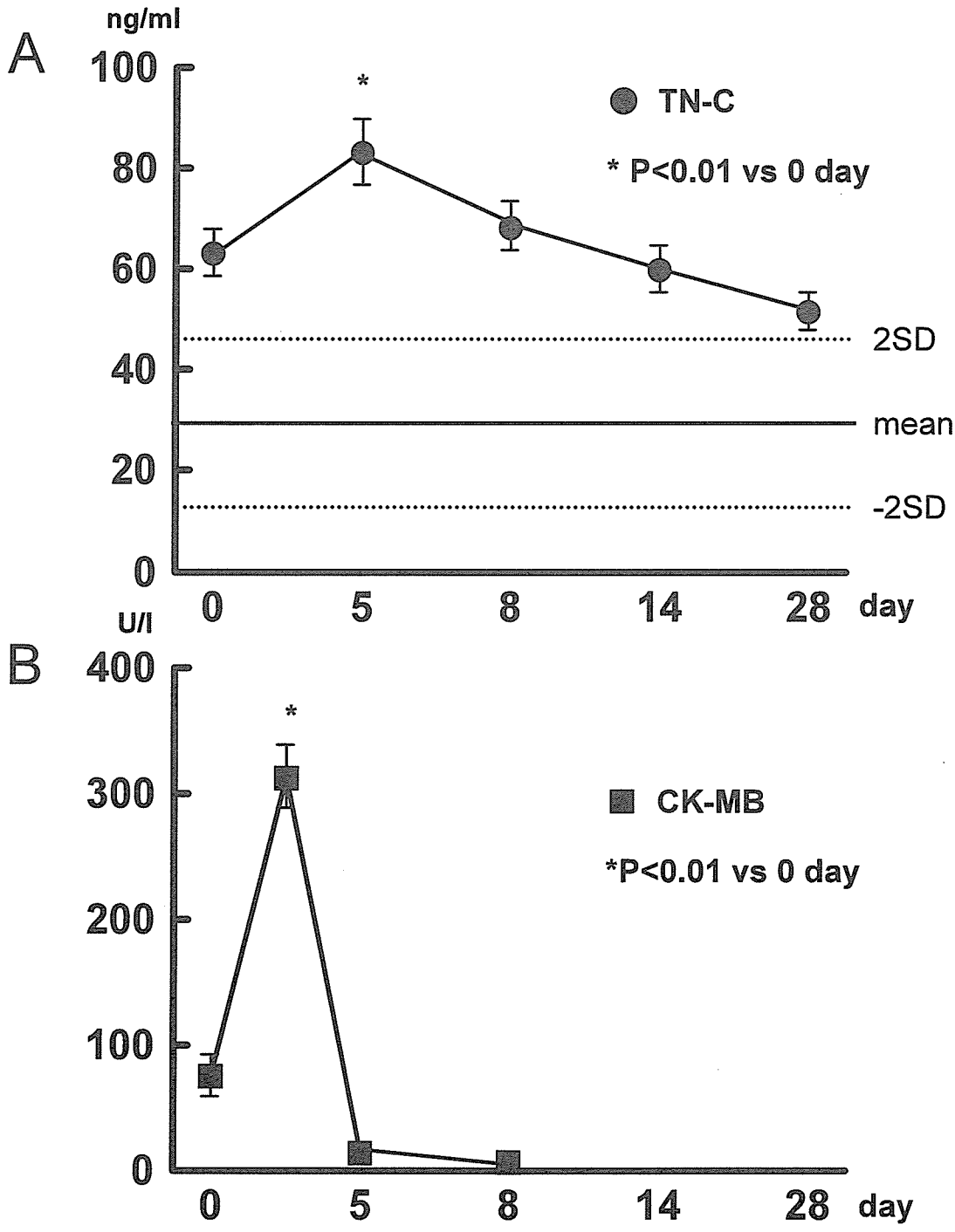
A
ng/ml
100
80
60
40
20
0
*
TN-C
* P<0.01 vs 0 day
2SD
mean
-2SD
0
5
8
14
28
day
B
U/l
400
300
200
100
0
*
CK-MB
*P<0.01 vs 0 day
0
5
8
14
28
day

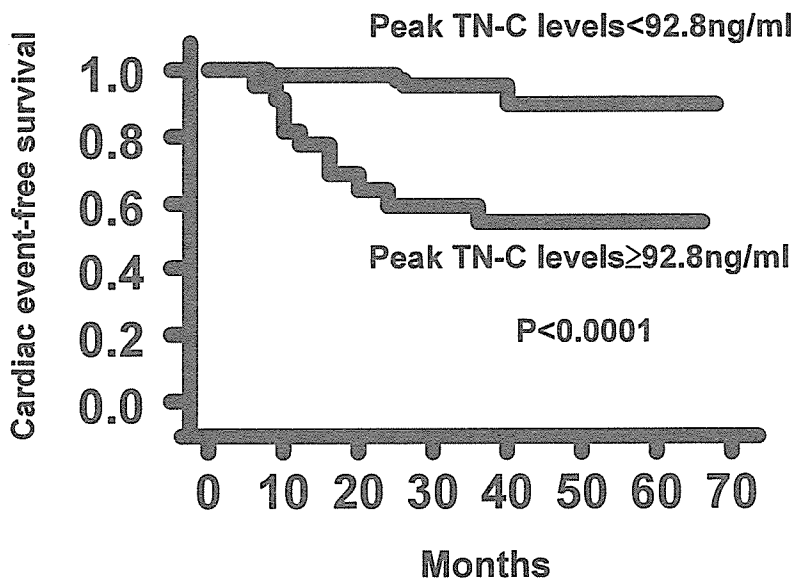
Peak TN-C levels<92.8ng/ml
Peak TN-C levels≥92.8ng/ml
P<0.0001
Cardiac event-free survival
1.0
0.8
0.6
0.4
0.2
0.0
0 10 20 30 40 50 60 70
Months

Available online at www.sciencedirect.com
SCIENCE DIRECT
Biochemical and Biophysical Research Communications 342 (2006) 379–386
BBRC
www.elsevier.com/locate/ybbrc

αB-crystallin mutation in dilated cardiomyopathy

Natsuko Inagaki [a,b], Takeharu Hayashi [a], Takuro Arimura [a], Yoshinori Koga [c], Megumi Takahashi [a], Hiroki Shibata [a], Kunihiko Teraoka [b], Taishiro Chikamori [b], Akira Yamashina [b], Akinori Kimura [a,*]

[a] *Department of Molecular Pathogenesis, Medical Research Institute and Laboratory of Genome Diversity, School of Biomedical Science, Tokyo Medical and Dental University, Tokyo 101-0062, Japan*
[b] *Second Department of Internal Medicine, Tokyo Medical University, Tokyo 160-0023, Japan*
[c] *Department of Cardiovascular Medicine, Kurume University Medical Center, Kurume 839-0863, Japan*

Received 16 January 2006
Available online 8 February 2006

Abstract

Mutations in genes for sarcomeric proteins such as titin/connectin are known to cause dilated cardiomyopathy (DCM). However, disease-causing mutations can be identified only in a small proportion of the patients even in the familial cases, suggesting that there remains yet unidentified disease-causing gene(s) for DCM. To explore the novel disease gene for DCM, we examined *CRYAB* encoding αB-crystallin for mutation in the patients with DCM, since αB-crystallin was recently reported to associate with the heart-specific N2B domain and adjacent I26/I27 domain of titin/connectin, and we previously reported a N2B mutation, Gln4053ter, in DCM. A missense mutation of *CRYAB*, Arg157His, was found in a familial DCM patient and the mutation affected the evolutionary conserved amino acid residue among α-crystallins. Functional analysis revealed that the mutation decreased the binding to titin/connectin heart-specific N2B domain without affecting distribution of the mutant crystallin protein in cardiomyocytes. In contrast, another *CRYAB* mutation, Arg120Gly, reported in desmin-related myopathy decreased the binding to both N2B and striated muscle-specific I26/27 domains and showed intracellular aggregates of the mutant protein. These observations suggest that the Arg157His mutation may be involved in the pathogenesis of DCM via impaired accommodation to the heart-specific N2B domain of titin/connectin and its disease-causing mechanism is different from the mutation found in desmin-related myopathy.

Keywords: Dilated cardiomyopathy; Desmin-related myopathy; αB-crystallin; Titin/connectin; Mutation

Dilated cardiomyopathy (DCM) is a disease of unknown etiology characterized by cardiac enlargement accompanied by systolic dysfunction and often manifested with congestive heart failure [1]. Although the majority of DCM patients are sporadic cases and may be caused by extrinsic factors such as ischemia and metabolic disease, family histories can be found in 20–35% of patients, suggesting that intrinsic factors or genetic abnormalities cause DCM at least in a part of the patients [2]. There are several reports on the gene mutations in DCM, and the genetic etiologies of DCM may be classified into at least five groups: (1) abnormalities in the components for cytoarchitecture of cardiomyocytes, such as mutations in genes for α-cardiac actin, desmin, dystrophin, δ-sarcoglycan, metavinculin, titin/connectin, muscle LIM protein (MLP), T-cap/telethonin, and Cypher/ZASP [3–11], (2) mutations in the genes for sarcomeric proteins of the heart, such as cardiac β-myosin heavy chain and cardiac troponin T [12], (3) mutations affecting supply and/or regulation of energy demand, such as CPTase II deficiency, tafazzin gene mutations, and recently reported *ABCC9* mutations [13–15], (4) defects in the component of nuclear envelope, which may participate in signal transduction between the cytoplasm and the nucleus, such as mutations in lamin A/C gene [16], and (5) cardiac ion channel mutations [17]. In addition, mutation of a transcriptional coactivator was

* Corresponding author. Fax: +81 3 5280 8055.
E-mail address: akitis@mri.tmd.ac.jp (A. Kimura).

0006-291X/$ - see front matter © 2006 Elsevier Inc. All rights reserved.
doi:10.1016/j.bbrc.2006.01.154

recently reported to cause DCM accompanied by hearing loss [18].

Among these genetic causes, the majority can be classified into the cytoarchitectural abnormalities that may cause abnormal force transmission across the Z-line between the sarcomere [19]. The disease-causing mutations in cytoarchitectural components are in general found in the heterozygous state (exception is the dystrophin mutation that can be found in hemizygous state in male patient), and hence the disease is inherited as autosomal dominant genetic trait. The genetic defects or mutations in the disease genes, however, could be identified only in a minor proportion of DCM patients, even if they have apparent family histories, i.e., familial DCM patients. On the other hand, linkage studies suggested many different disease loci in different multiplex families with DCM. These observations indicate that there are many other disease genes to be identified for better understanding the molecular pathogenesis of DCM.

αB-crystallin is one of several crystallins in the vertebrate lens [20], but can be found in tissues other than lens, including cardiac and skeletal muscles. Content of αB-crystallin in cardiac muscle is 3–5% of the total soluble protein [21], and the muscle fibers are protected from the effect of ischemia, preventing extensive structural damage, by the αB-crystallin [22–24]. It was reported that the αB-crystallin moved from cytosol to myofibrils following ischemia [25]. Immunoelectron microscopic analysis of rat hearts has shown that αB-crystallin can be found in a narrow region of the I-band rather than in the Z-disc and is associated with desmin filaments connecting neighboring myofibrils [26]. Recently, mutations in the gene for αB-crystallin (*CRYAB*) were reported in striated muscle disorder including desmin-related myopathy (DRM), characterized by skeletal muscle weakness associated with cardiomyopathy [27,28]. These observations suggested the important role of αB-crystallin in biological function of striated muscles on the physiological and pathological conditions. In addition, it was recently reported that the αB-crystallin bound titin/connectin in the I-band region, more specifically at the N2B and I26/I27 domains, and this was supported by both co-purification and co-localization of αB-crystallin with titin/connectin [26,29].

Titin/connectin is a giant muscle protein expressed in the cardiac and skeletal muscles, spanning entire half of the sarcomere from Z-line to M-line, and plays a key role in muscle assembly, force transmission at the Z-line, and maintenance of resting tension in the I-band region [30,31]. We and others have recently reported several mutations in the titin/connectin gene (*TTN*) associated with cardiomyopathy [8,32], including a DCM-associated nonsense mutation, Gln4053ter, and another missense mutation, Ser3799Tyr, found in hypertrophic cardiomyopathy (HCM), at the N2B domain of titin/connectin in the I-band region [8] where αB-crystallin interacts with titin/connectin [29]. Since the N2B domain is expressed only in the cardiac muscle [30,31], its mutation as well as mutation of its associated protein such as αB-crystallin might cause cardiac muscle disease. It is then of interest to search for *CRYAB* mutations in DCM as well as to investigate whether the cardiomyopathy associated *TTN* mutations would affect the binding to αB-crystallin.

In this study, a novel *CRYAB* mutation was found in familial DCM and its functional alteration was investigated along with the DRM-causing mutation. This is the first report of DCM-associated *CRYAB* mutation which showed different functional alteration from the DRM-associated mutation.

Materials and methods

Subjects. One hundred and thirty genetically unrelated Japanese patients with DCM were chosen as subjects. Among them, a family history of the disease was observed in 36 cases. All the patients manifested with typical DCM phenotype as described previously [11,33]. These patients had been analyzed for mutations and no mutations were found in any genes. Control subjects were 200 unrelated healthy Japanese individuals selected at random. After acquiring informed consent, blood samples were obtained from each subject. The protocol for research was approved by the Ethics Reviewing Committee of Medical Research Institute, Tokyo Medical and Dental University.

Genomic DNA extraction and mutational analysis of CRYAB. Genomic DNA extracted from peripheral blood of each panels was subjected to polymerase chain reaction (PCR) under standard conditions by using of primer pairs specific to each region analyzed. Sequence information for the primers is as follows: 1F, 5′-CTGTAGCTGCAGCTGAAGG-3′; 1R, 5′-CAGGAGGTTCCAGTAAGGAC-3′; 2F, 5′-AGACAGCACCTGT GTAATCAG-3′; 2R, 5′-GCACTACCTGGACTATTACAG-3′; 3F, 5′-CTCTCTGCCTCTTTCCTCAT-3′; 3R, 5′-GTCACAAGACTTTCATT CACTG-3′. The PCR was performed separately with combinations of primers, 1F and 1R, 2F and 2R, and 3F and 3R. The PCR products from patients were sequenced from the primers on both strands.

Amino acid sequence comparison of αA-crystallin and αB-crystallin from various species. Protein sequence of human αB-crystallin predicted from nucleotide sequence (GenBank Accession No. NM_001885) was aligned with those of macaque (AB125159), elephant (AJ617732), bovine (NM_174290), sheep (AY819023), dog (XM_536576), rat (NM_012935), mouse (NM_009964), duck (U16124), chicken (U26661) and zebrafish (NM_131157), along with αA-crystallin sequences from human (NM_000394), bovine (NM_174289), sheep (AY819022), rat (NM_012534), mouse (NM_013501), platypus (AJ617724), lizard (AJ617726), cavefish (Y11301), and zebrafish (BC083177). The predicted translation from mRNAs to proteins and alignment was performed using DNASIS Software (Hitachi).

Mammalian two-hybrid (M2H) assays for binding affinity between αB-crystallin and titin/connectin. Human *CRYAB* cDNA fragments (GenBank Accession No. NM_001885, nucleotides 26–550) were amplified from cardiac total RNA by using the RT-PCR method. A wild-type (WT) cDNA fragment was obtained by using primers CRYAB-2H-SalF (5′-GTCGACTTATGGACATCGCCATCCACCACCCCTGGATC-3′, underlined sequences are added for cloning) and CRYAB-2H-NotR (5′-GCGGCCGCTTTCTTGGGGGCTGCGGTGACAGCAGGCTTC TCTT-3′). Two equivalent mutant cDNA fragments having G to A (DCM associated Arg157His mutation) or A to G (DRM-associated Arg120Gly mutation) substitutions introduced by primer-directed mutagenesis method were obtained by using combinations of the following primers, CRYAB-2H-SalF and CRYAB-157HF (5′-GCCCTGAGCaCACCA TTCCCATCACCCGTG-3′, lowercase letter is the mutation to be introduced) with CRYAB-157HR (5′-GGGAATGGTGtGCTCAGGGC CAGAGACCTG-3′) and CRYAB-2H-NotR for the Arg157His mutation, and CRYAB-2H-SalF and CRYAB-R120GF (5′-GAGTTCCACgG GAAATACCGGATC-3′) with CRYAB-R120GR (5′-GATCCGGTAT TTCCcGTGGAACTC-3′) and CRYAB-2H-NotR for the Arg120Gly mutation, respectively. *TTN* cDNA fragments encoding N2B (X90568, nucleotides 11,379–12,189) or I26/I27 domains (X90568, nucleotides

12,849–13,416) were obtained using the following primers: N2B-SalF (5′-GTCGACTTGAATTGCAATCCATTTTGGAG-3′) and N2B-NotR (5′-GCGGCCGCGCTTTCCTTAGAAAGAAGGTC-3′) (for N2B domain); I26/I27-2H-SalF (5′-GTCGACTTGAGGATGGCCCCATGATACATA CACCTTTA-3′) and I26/I27-2H-NotR (5′-GCGGCCGCCACTGT CACAGTTAGTGTGGCTGTACACCTGACACTG-3′) (for I26/I27 domain), respectively. The DCM or HCM-associated *TTN* mutations (Gln4053ter or Ser3799Tyr, respectively) [8] were introduced into the TTN cDNA fragment by primer-mediated mutagenesis method. The following primers were used; N2B-SalF and N2BinM2R (5′-CTGTACCTCCTa CACTTTCT-3′) in combination with N2BinM2F (5′-AGAAAG TGtAGGAGGTACAG-3′) and N2B-NotR for the Gln4053ter mutation. N2B-HCMmutF (5′-GTCGACTTGAATTGCAATaCATTTTGGAG-3′) and N2B-NotR were used to obtain a cDNA clone for the Ser3799Tyr mutation. All cDNA fragments were cloned into pCRII (Invitrogen), sequenced to confirm that no PCR errors were introduced, and excised by digestion by *Sal*I and *Not*I. The excised cDNA fragments were then cloned into the p-ACT vector containing pVP16 as a prey (for *TTN* cDNAs) and the p-BIND vector containing pGAL4 as a bait (for *CRYAB* cDNAs) (CheckMate Mammalian two-hybrid system, Promega). These constructs were sequenced to ensure that no errors were introduced.

HeLa cells were grown in Dulbecco's modified Eagle's medium (DMEM) supplemented with 10% fetal bovine serum (FBS) and 1% penicillin/streptomycin at 37 °C with 5% CO_2. Cells were seeded at 1.0×10^6/well in six-well plates 24 h before the transfection. 0.3 μg each of the p-ACT-based plasmids and the p-BIND-based plasmids was co-transfected along with pG5*luc* vectors into HeLa cells by 1.8 μl of TransFectin Lipid Reagent (Bio-Rad) per well. The transfected cells were cultured again for 24 h at 37 °C in 5% CO_2 and the cells were lysed to measure the amount of *Firefly* and *Renilla reniformis* luciferase activities using the Dual-Luciferase Reporter Assay System (Promega) according to the manufacturer's instruction. At least four experiments were performed for each combination of constructs. The *Firefly* luciferase activities were corrected by *R. reniformis* luciferase activities which normalize the transfection efficiency and the arbitrarily units (AU) were expressed as means ± standard deviation (SD). Statistical differences were examined by Student's *t* test and *p* values of less than 0.05 were considered to be statistically significance. Cells co-transfected in a combination of p-ACT-*TTN* cDNA-based plasmids and only p-BIND vectors, or only p-ACT vectors and p-BIND-*CRYAB* cDNA-based plasmids expressed virtually no luciferase activity, showing no self-activation in our system.

Cell culture and transfection procedures. Neonatal cardiomyocytes were isolated from one or two days of age Sprague–Dawley rats by repetitive digestion with 0.2% collagenase type II (Worthington) and purified by discontinuous gradient method with Percoll [34]. 2×10^5 cells were plated on the collagen-I-coated 8-well coverslips (Beckton–Dickinson) in DMEM containing 10% FBS and 1% penicillin/streptomycin for 24 h. For transient transfection into neonatal cardiomyocytes, 0.4 μg of p-BIND-based constructs (*CRYAB* WT, R157H or R120G) was added into each well with 0.8 μl of TransFectin Lipid Reagent. Twenty-four hours after the transfection, cardiomyocytes were washed, fixed, and stained as described in the following section.

Immunohistochemical analysis. Transfected rat cardiomyocytes were fixed for 10 min in 100% ethanol at −20 °C and incubated for 1 h with 3% bovine serum albumin in phosphate-buffered saline at room temperature. The primary and secondary antibodies used were mouse anti-GAL4 monoclonal antibody (Santa Cruz) and Alexa fluor 568 goat anti-mouse IgG (Molecular Probes), respectively. Immunofluorescence microscopy was performed using a laser confocal microscope (Axioplan2 MOT; Carl Zeiss).

Results

Identification of a missense mutation in CRYAB in DCM

Sequence variations in *CRYAB* were searched for in the Japanese DCM patients using the direct sequence method. We found a T to G transition in an intron (+4 in intron 2) and a heterozygous missense mutation (CGC to CAC at codon 157 in exon 3, replacing arginine with histidine, Arg157His, Fig. 1A) in the DCM population. While the former transition was found in many patients, the missense mutation was found only in a 71-year-old female patient (CM191) who had apparent family history. The Arg157His mutation was not found in 400 control chromosomes and the mutated residue was evolutionary conserved in αB- and αA-crystallin from various species (Fig. 1B). Clinical manifestations of this patient were mild and had been slowly expressed; she developed cardiac symptoms only

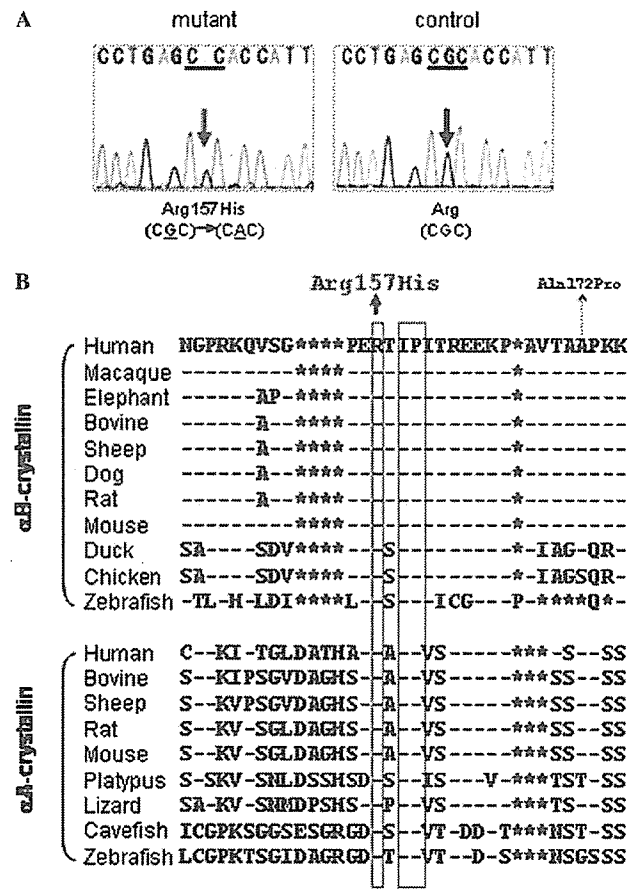

Fig. 1. Mutational analysis of *CRYAB* in DCM. (A) Direct sequencing data of CRYAB exon 3 from a control (left) and the proband (right). Codon 157 of the control was CGC (Arg), whereas the patient was heterozygous for a CAC (His) mutation. (B) Protein sequence of human αB-crystallin predicted from nucleotide sequence (GenBank Accession No. NM_001885) was aligned with those of macaque (AB125159), elephant (AJ617732), bovine (NM_174290), sheep (AY819023), dog (XM_536576), rat (NM_012935), mouse (NM_009964), duck (U16124), chicken (U26661), and zebrafish (NM_131157), along with αA-crystallin sequences from human (NM_000394), bovine (NM_174289), sheep (AY819022), rat (NM_012534), mouse (NM_013501), platypus (AJ617724), lizard (AJ617726), cavefish (Y11301), and zebrafish (BC083177). Boxs indicate evolutionary highly conserved residues in the proteins from various species. Dashes indicate identities to the human αB-crystallin sequence. The DCM-associated His157Arg mutation found in this study and a sequence variation found in database (Ala172Pro) are indicated. *indicates spaces introduced to maximize the homology.

after fourth decade. Her electrocardiogram showed apparent inverted T waves in V4–V6 leads and ventricular tachycardia (data not shown). She had six siblings; two of them (56 year and 66 year) were affected with DCM and sudden cardiac death was observed in the other two siblings (at the age of 60 year and 72 year). It was, however, not clear whether these siblings had the mutation or not, because three of them had died and genetic testing was refused by the other one.

Difference between DCM- and DRM-associated CRYAB mutations in regard to the cytoplasmic distribution in neonatal rat cardiomyocytes

Since the DRM-associated *CRYAB* mutation, Arg120-Gly was reported to cause aggregation of mutant protein in cells [27], we investigated the cellular distribution of Arg157His mutant αB-crystallin protein as compared with the Arg120Gly mutant. For this purpose, rat primary cardiomyocytes were transfected with the p-BIND based *GAL4-CRYAB* constructs with or without the mutations and the transiently expressed GAL4 fusion proteins in cells were detected by anti-GAL4 antibody under a confocal microscope (Fig. 2). The GAL4 signals fused to the DRM-associated Arg120Gly mutation showed apparent cytoplasmic GAL4-αB-crystallin-labeled aggregates in almost all cells producing GAL4-αB-crystallin, which was consistent with previous report [27]. On the other hand, the GAL4 signals fused to the DCM-associated Arg157His mutation were distributed throughout the cytoplasm and showed similar localization as compared to that of GAL4-*CRYAB* WT.

Functional alterations in binding of αB-crystallin and titin/connectin caused by the mutations

To further explore the functional changes caused by the DCM-associated Arg157His mutation or DRM-associated Arg120Gly mutation in binding αB-crystallin at the N2B and I26/I27 domains of titin/connectin, we performed mammalian-two-hybrid (M2H) assays. A bait plasmid containing WT or mutant *CRYAB* cDNA was co-transfected with a prey plasmid containing *TTN* cDNA corresponding to N2B or I26/I27 domains of titin/connectin. As shown in Fig. 3, the luciferase activity in the transfectants containing the WT *TTN*-N2B construct with the DCM-associated or DRM-associated mutant *CRYAB* constructs (0.25 ± 0.029 or 0.13 ± 0.027 AU, respectively) was significantly lower than those of WT *TTN*-N2B and WT *CRYAB* (1.00 ± 0.14 AU, $p < 0.001$ in each case) (Fig. 3A). The luciferase activity in the transfectants of the DCM-associated mutant *CRYAB* with *TTN*-I26/I27 (0.13 ± 0.066 AU) was slightly lower than those of WT *CRYAB* and *TTN*-I26/I27 (0.19 ± 0.060 AU), but the difference did not reach statistical significance ($p = 0.23$) (Fig. 3B). In contrast, the luciferase activity in the transfectants of DRM-associated mutant *CRYAB* and WT *TTN*-N2B (0.073 ± 0.015 AU) was significantly lower than those of WT *CRYAB* and WT *TTN*-N2B ($p < 0.01$) (Fig. 3B). Negative controls containing either αB-crystallin or titin/connectin plasmids showed only little and negligible luciferase activity indicating no self-activation in these constructs.

Because the alteration of binding between αB-crystallin and titin/connectin N2B domain may play an important role in developing cardiomyopathy, we investigated by using the M2H assay whether the DCM-associated Gln4053ter mutation and HCM-associated Ser3799Tyr mutation in the N2B domain of titin/connectin [8] would affect binding to αB-crystallin. It was shown that the luciferase activity obtained from transfectants containing WT *CRYAB* with Gln4053ter *TTN*-N2B was 0.16 ± 0.012 AU, which was significantly lower than those for WT *CRYAB* and WT *TTN*-N2B ($p < 0.001$, Fig. 3A). Quite interestingly, the HCM-associated Ser3799Tyr mutation also significantly decreased the luciferase activity (0.37 ± 0.001 AU, $p < 0.001$, Fig. 3A) albeit to a lesser extent than the DCM-associated Gln4053ter mutation.

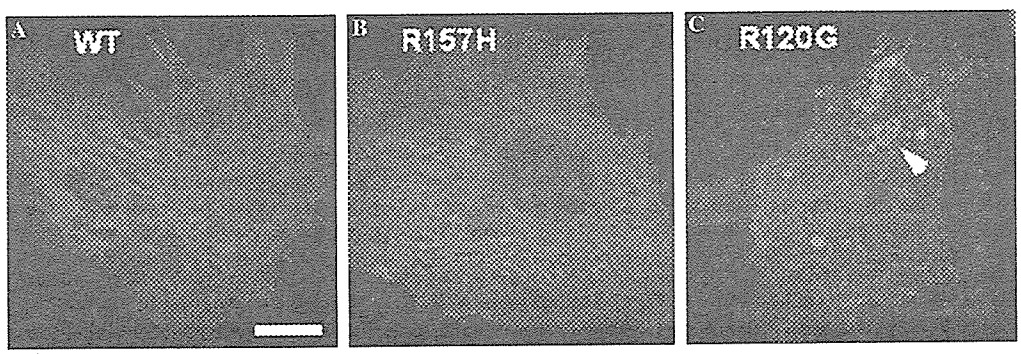

Fig. 2. Fluorescence images of transiently expressed (A) wild-type (WT) and mutant αB-crystallin fused to pGAL4. Twenty-four hours after transfection with each construct, rat cardiomyocytes were processed for indirect immunofluorescence to detect the distribution of GAL4-tagged αB-crystallin. The localization of (B) αB-crystallin R157H (Arg157Hs) was similar to that of αB-crystallin WT in rat neonatal cardiomyocytes. In contrast, aggregates (white arrowhead) were detected by the GAL4 antibody in the cardiomyocytes transfected with (C) R120G (Arg120Gly) αB-crystallin cDNA. Bar, 10 μm.

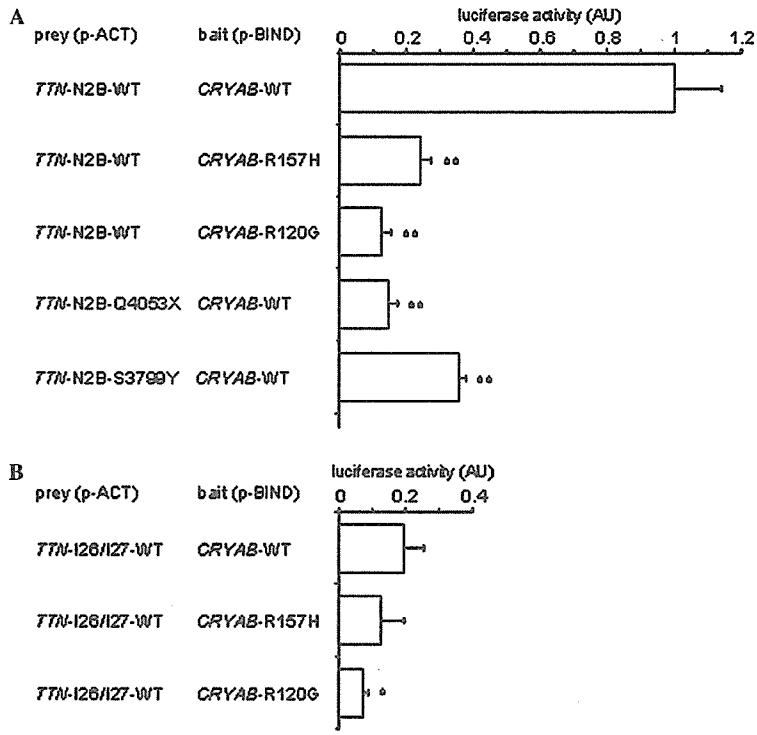

Fig. 3. Binding of αB-crystallin with titin/connectin in the presence of DCM or DRM-associated mutations. Luciferase activities obtained in the M2H assay. Data are represented as means ± SD ($n = 4$ for each case). *$p < 0.01$ vs WT; **$p < 0.001$ vs WT. (A) Binding pairs are titin/connectin N2B domain wild-type (WT) with αB-crystallin WT, αB-crystallin R157H (Arg157His) or αB-crystallin R120G (Arg120Gly) mutants, and titin/connectin N2B domain Q4053X (Gln4053ter) or S3799Y (Ser3799Tyr) mutants with αB-crystallin WT. (B) Binding pairs are titin/connectin I26/I27 domain with αB-crystallin WT, αB-crystallin R157H or αB-crystallin R120G mutants.

Discussion

We report here a *CRYAB* mutation, Arg157His, found in a late-onset DCM patient. The mutation affected the evolutionary conserved amino acid residue of crystallins and not detected in 200 healthy controls. We could not exclude a possibility that the Arg157His mutation might be a rare polymorphism not associated with DCM. However, upon searching for sequence variations of human *CRYAB* in the literature and public databases (UCSC genome browser, NCBI OMIM, and Entrez SNP), we found five non-synonymous sequence variations, Glu30ter (from AAG to TAG at codon 30; rs11549440), Ser41Tyr (from TCT to TAT at codon 41, rs2234703), Pro51Leu (from CCA to CTA at codon 51; rs2234740), Arg120Gly (from CGC to CAC at codon 129; rs28929489), and Ala172Pro (from GCC to CCC at codon 172; rs11549441). Ser41Tyr and Pro51Leu are polymorphisms confirmed for the presence, and the Arg120Gly was a disease-causing mutation found in DRM [27]. When we aligned amino acid sequences of αB-crystallin and αA-crystallin from various species, Ser41, Pro51, and Ala172 were not evolutionary conserved (Figs. 1 and 4), whereas Arg120 was completely conserved (Fig. 4), suggesting the functional importance of Arg120. On the other hand, Glu30 was also well conserved, but the Glu30ter variation should encode for a truncated crystallin protein that will cause αB-crystallopathy such as DRM (OMIM 608810, 123590). Since the Glu30ter and Ala172Pro variations were found only in the Cerela's mRNA data and not confirmed for the presence in human genome, these variations might be sequence artifacts. In this study, we demonstrated that the *CRYAB* mutation caused functional alteration such that the mutation reduced the binding of αB-crystallin to the N2B domain, but not to I26/I27domain, of titin/connectin. In addition, we showed that the DCM-associated *TTN* mutation in the N2B domain, Gln4053ter, also reduced the binding of titin/connectin to αB-crystallin. These observations suggested that the *CRYAB* Arg157His mutation was associated with DCM and not a simple polymorphism.

αB-crystallin serves as chaperone belonging to the low-molecular-weight heat shock proteins present in the highest quantities in heart [21]. It was demonstrated from studies of αB-crystallin knock-out and overexpression mice that αB-crystallin plays protective roles against ischemia-reperfusion-induced damage such as impaired cardiac contractility as well as increased necrosis and apoptosis [24,35]. The translocation of αB-crystallin from cytosol to myofibrils, especially to a narrow region of the I-band during cardiac ischemia, has been reported and may be related with its protective role [25,26]. In addition, αB-crystallin has recently been shown to associate with the I-band region of titin/connectin [26,29]. Because both αB-crystallin and titin/connectin mutations found in DCM reduced binding

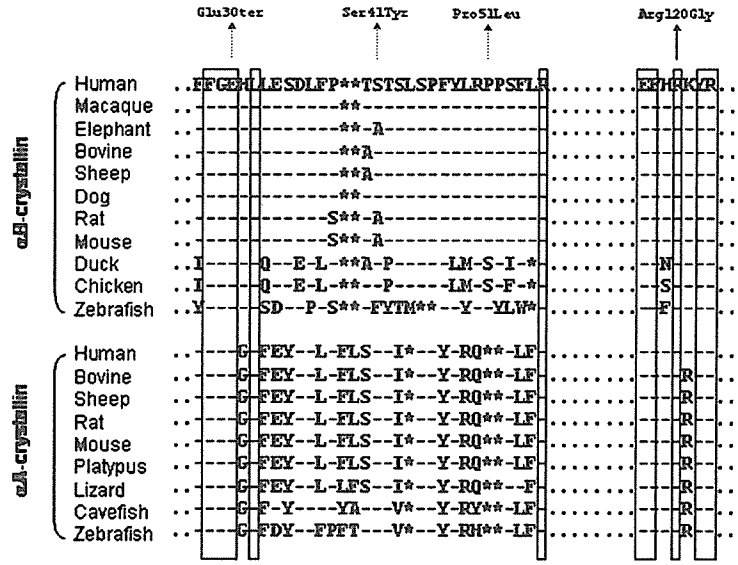

Fig. 4. Amino acid sequence alignment of a-crystallins from various species and variations found in database. Protein sequence of α-crystallins from various species was predicted from nucleotide sequence as described in Fig. 1. Sequence variation found in database (Glu30ter, Ser41Tyr, and Pro51Leu) and the disease-causing mutation reported for DRM (Arg120Gly) is indicated. Boxes indicate evolutionary highly conserved residues in the proteins from various species. Dashes, dots, and stars indicate identity to human αB-crystallin, not shown, and spaces introduced to obtain maximum homology, respectively.

interaction between the heart-specific N2B domain of titin/connectin and αB-crystallin, it was speculated that the impaired localization of αB-crystallin into the I-band region of cardiac muscle may predispose early progression to heart failure under the stressed condition. This may be consistent with late-onset nature of DCM associated with the *CRYAB* mutation. It was of interest that the HCM-associated *TTN*-N2B mutation also showed decreased binding to αB-crystallin. It is not clear the mechanism of decreased binding of titin/connectin N2B region and αB-crystallin in developing different clinical phenotypes of cardiomyopathy, but the DCM-associated *TTN* mutation affected the binding more severely than the HCM-associated mutation, suggesting that more severe functional change might cause earlier decompensation of ventricular function.

A number of muscular dystrophy and isolated DCM are caused by mutations in the same disease genes. Although the cardiac involvement, DCM-like phenotype, is often found in the patients with muscular dystrophy caused by the disease gene mutations, a part of the DCM patients carrying the disease gene mutations are affected without skeletal muscle phenotype. The etiological link between hereditary cardiomyopathy and inherited striated muscle myopathy has led to a question as how the mutations in the genes/proteins expressed in both skeletal and cardiac muscles cause heart specific disease, isolated DCM. The most probable explanation is that the difference in the clinical phenotypes, muscular dystrophy and DCM, can be caused by mutations in different functional domains affecting different functions. In this study, the Arg157His mutant αB-crystallin showed decreased binding to the I-band region of titin/connectin in the M2H assay. Interestingly, the altered binding was observed with the cardiac-specific N2B domain but not with the I26/I27 domain which is just near the N2B domain and expressed in both skeletal muscle and cardiac muscle, and these functional alterations were not associated with the formation of mutant protein aggregates. In contrast, the Arg120Gly mutation that was identified in a family with DRM [27] decreased binding to both N2B and I26/I27 domain and led to the accumulation of mutant αB-crystallin aggregates. It was also reported that the Arg120Gly mutation decreased binding to striated muscle-specific desmin filament and promoted aggregation of desmin filament [36]. The reason why the *CRYAB* Arg157His mutation caused cardiac muscle dysfunction but not the skeletal muscle myopathy may be due to the cardiac-specific functional alteration. In addition, the Arg120Gly mutation showed a dominant-negative effect in promoting aggregation of desmin [36], while the Arg157His mutation was not expected to show dominant-negative effect since the binding ratio of αB-crystallin and titin/connectin was assumed to be 1:1 [29] and the *CRYAB* Arg157His mutant protein did not generate any aggregations in cardiomyocytes as demonstrated in this study. Moreover, because a subtle functional change of striated muscle-associated molecule could affect only the cardiac muscle, while the skeletal muscle would be affected by more severe functional change, as reported for caveolin-3 mutations [37], theoretical functional loss of αB-crystallin in heterozygous carrier of the Arg157His mutation (not less than half) might be enough to affect the function of cardiac muscle. These differences in the nature of mutational effect might also contribute to the difference in affected muscles

by these mutations, although the causative role of Arg157His mutation should be tested directly such that heterozygous knock-in mice of *CRYAB* Arg157His mutation would develop DCM.

Titin/connectin is the so far known largest (~3 MDa) protein expressed in the striated muscle, and arranged in an anti-parallel manner to span the entire sarcomere, with their amino- and carboxyl-terminal ends in the Z- and M-lines, respectively [30,31]. Titin/connectin appears to be a key component in the assembly and function of vertebrate striated muscles, i.e., it has an important role as anchoring protein for the other sarcomere/Z-disc proteins [30]. Indeed, the abnormalities of titin itself and titin-associated proteins such as cardiac myosin-binding protein-C, α-actinin, and T-cap/telethonin cause DCM [8,9,32,38,39], despite the fact that the functional alteration in "titin-related cardiomyopathy" may depend on the mutations in each gene. Here, we propose that the genes encoding for titin-associated proteins are good candidates of novel disease genes for DCM. For example, a recent report shows that the heart-specific N2B domain of titin/connectin binds to four and half LIM protein 2 (*FHL2*) which tethers the metabolic enzymes such as adenylate kinase, phosphofructokinase, and muscle creatinine kinase [40], implying that *FHL2* can be a candidate disease gene for DCM.

Acknowledgments

We are grateful to Drs. H. Toshima, H. Nishi, K. Matsuyama, H. Kagiyama, T. Sakamoto, K. Kawai, K. Kawamura, R. Kusukawa, M. Nagano, Y. Nimura, R. Okada, T. Sugimoto, H. Tanaka, H. Yasuda, F. Numano, K. Fukuda, S. Ogawa, A. Matsumori, S. Sasayama, R. Nagai, and Y. Yazaki for their contributions to clinical evaluation and blood sampling from patients with DCM. We also thank Dr. M. Yanokura, and Ms. M. Emura for their technical assistance. This work was supported in part by Grants-in-Aid from the Ministry of Education, Culture, Sports, Science and Technology, Japan, a research grant from the Ministry of Health, Labour and Welfare, Japan, and research grants from Kurozumi Medical Foundation, Mochida Memorial Foundation for Medical and Pharmaceutical Research, and Mitsubishi Pharma Research Foundation.

References

[1] P. Richardson, W. McKenna, M. Bristow, B. Maisch, B. Mautner, J. O'Connell, E. Olsen, G. Thiene, J. Goodwin, I. Gyarfas, I. Martin, P. Nordet, Report of the 1995 World Health Organization/International Society and Federation of Cardiology Task Force on the Definition and Classification of Cardiomyopathies, Circulation 93 (1996) 841–842.

[2] V.V. Michels, P.P. Moll, F.A. Miller, A.J. Tajik, J.S. Chu, D.J. Driscoll, J.C. Burnett, R.J. Rodeheffer, J.H. Chesebro, H.D. Tazelaar, The frequency of familial dilated cardiomyopathy in a series of patients with idiopathic dilated cardiomyopathy, N. Engl. J. Med. 326 (1992) 77–82.

[3] T.M. Olson, V.V. Michels, S.N. Thibodeau, Y.S. Tai, M.T. Keating, Actin mutations in dilated cardiomyopathy, a heritable form of heart failure, Science 280 (1998) 750–752.

[4] D. Li, T. Tapscoft, O. Gonzalez, P.E. Burch, M.A. Quinones, W.A. Zoghbi, R. Hill, L.L. Bachinski, D.L. Mann, R. Roberts, Desmin mutation responsible for idiopathic dilated cardiomyopathy, Circulation 100 (1999) 461–464.

[5] F. Muntoni, M. Cau, A. Ganau, R. Congiu, G. Arvedi, A. Mateddu, M.G. Marrosu, C. Cianchetti, G. Realdi, A. Cao, et al., Brief report: deletion of the dystrophin muscle-promoter region associated with X-linked dilated cardiomyopathy, N. Engl. J. Med. 329 (1993) 921–925.

[6] S. Tsubata, K.R. Bowles, M. Vatta, C. Zintz, J. Titus, L. Muhonen, N.E. Bowles, J.A. Towbin, Mutations in the human delta-sarcoglycan gene in familial and sporadic dilated cardiomyopathy, J. Clin. Invest. 106 (2000) 655–662.

[7] T.M. Olson, S. Illenberger, N.Y. Kishimoto, S. Huttelmaier, M.T. Keating, B.M. Jockusch, Metavinculin mutations alter actin interaction in dilated cardiomyopathy, Circulation 105 (2002) 431–437.

[8] M. Itoh-Satoh, T. Hayashi, H. Nishi, Y. Koga, T. Arimura, T. Koyanagi, M. Takahashi, S. Hohda, K. Ueda, T. Nouchi, M. Hiroe, F. Marumo, T. Imaizumi, M. Yasunami, A. Kimura, Titin mutations as the molecular basis for dilated cardiomyopathy, Biochem. Biophys. Res. Commun. 291 (2002) 385–393.

[9] R. Knoll, M. Hoshijima, H.M. Hoffman, V. Person, I. Lorenzen-Schmidt, M.L. Bang, T. Hayashi, N. Shiga, H. Yasukawa, W. Schaper, W. McKenna, M. Yokoyama, N.J. Schork, J.H. Omens, A.D. McCulloch, A. Kimura, C.C. Gregorio, W. Poller, J. Schaper, H.P. Schultheiss, K.R. Chien, The cardiac mechanical stretch sensor machinery involves a Z disc complex that is defective in a subset of human dilated cardiomyopathy, Cell 111 (2002) 943–955.

[10] M. Vatta, B. Mohapatra, S. Jimenez, X. Sanchez, G. Faulkner, Z. Perles, G. Sinagra, J.H. Lin, T.M. Vu, Q. Zhou, K.R. Bowles, A. Di Lenarda, L. Schimmenti, M. Fox, M.A. Chrisco, R.T. Murphy, W. McKenna, P. Elliott, N.E. Bowles, J. Chen, G. Valle, J.A. Towbin, Mutations in Cypher/ZASP in patients with dilated cardiomyopathy and left ventricular non-compaction, J. Am. Coll. Cardiol. 42 (2003) 2014–2027.

[11] T. Arimura, T. Hayashi, H. Terada, S.Y. Lee, Q. Zhou, M. Takahashi, K. Ueda, T. Nouchi, S. Hohda, M. Shibutani, M. Hirose, J. Chen, J.E. Park, M. Yasunami, H. Hayashi, A. Kimura, A Cypher/ZASP mutation associated with dilated cardiomyopathy alters the binding affinity to protein kinase C, J. Biol. Chem. 279 (2004) 6746–6752.

[12] M. Kamisago, S.D. Sharma, S.R. DePalma, S. Solomon, P. Sharma, B. McDonough, L. Smoot, M.P. Mullen, P.K. Woolf, E.D. Wigle, J.G. Seidman, C.E. Seidman, Mutations in sarcomere protein genes as a cause of dilated cardiomyopathy, N. Engl. J. Med. 343 (2000) 1688–1696.

[13] I. Maurer, S. Zierz, Carnitine palmitoyltransferase in patients with cardiac ischemia due to atherosclerotic coronary artery disease and in patients with idiopathic dilated cardiomyopathy, Cardiology 88 (1997) 258–263.

[14] S. Bione, P. D'Adamo, E. Maestrini, A.K. Gedeon, P.A. Bolhuis, D. Toniolo, A novel X-linked gene, G4.5. is responsible for Barth syndrome, Nat. Genet. 12 (1996) 385–389.

[15] M. Bienengraeber, T.M. Olson, V.A. Selivanov, E.C. Kathmann, F. O'Cochlain, F. Gao, A.B. Karger, J.D. Ballew, D.M. Hodgson, L.V. Zingman, Y.P. Pang, A.E. Alekseev, A. Terzic, ABCC9 mutations identified in human dilated cardiomyopathy disrupt catalytic KATP channel gating, Nat. Genet. 36 (2004) 382–387.

[16] D. Fatkin, C. MacRae, T. Sasaki, M.R. Wolff, M. Porcu, M. Frenneaux, J. Atherton, H.J. Vidaillet Jr., S. Spudich, U. De Girolami, J.G. Seidman, C. Seidman, F. Muntoni, G. Muehle, W. Johnson, B. McDonough, Missense mutations in the rod domain of the lamin A/C gene as causes of dilated cardiomyopathy and conduction-system disease, N. Engl. J. Med. 341 (1999) 1715–1724.

[17] W.P. McNair, L. Ku, M.R. Taylor, P.R. Fain, D. Dao, E. Wolfel, L. Mestroni, SCN5A mutation associated with dilated cardiomyopathy,

conduction disorder, and arrhythmia, Circulation 110 (2004) 2163–2167.
[18] J. Schonberger, L. Wang, J.T. Shin, S.D. Kim, F.F. Depreux, H. Zhu, L. Zon, A. Pizard, J.B. Kim, C.A. Macrae, A.J. Mungall, J.G. Seidman, C.E. Seidman, Mutation in the transcriptional coactivator EYA4 causes dilated cardiomyopathy and sensorineural hearing loss, Nat. Genet. 37 (2005) 418–422.
[19] J.A. Towbin, The role of cytoskeletal proteins in cardiomyopathies, Curr. Opin. Cell Biol. 10 (1998) 131–139.
[20] S.P. Bhat, C.N. Nagineni, alpha B subunit of lens-specific protein alpha-crystallin is present in other ocular and non-ocular tissues, Biochem. Biophys. Res. Commun. 158 (1989) 319–325.
[21] J. Horwitz, The function of alpha-crystallin in vision, Semin. Cell Dev. Biol. 11 (2000) 53–60.
[22] J.L. Martin, R. Mestril, R. Hilal-Dandan, L.L. Brunton, W.H. Dillmann, Small heat shock proteins and protection against ischemic injury in cardiac myocytes, Circulation 96 (1997) 4343–4348.
[23] N. Golenhofen, P. Htun, W. Ness, R. Koob, W. Schaper, D. Drenckhahn, Binding of the stress protein alpha B-crystallin to cardiac myofibrils correlates with the degree of myocardial damage during ischemia/reperfusion in vivo, J. Mol. Cell Cardiol. 31 (1999) 569–580.
[24] P.S. Ray, J.L. Martin, E.A. Swanson, H. Otani, W.H. Dillmann, D.K. Das, Transgene overexpression of alphaB crystallin confers simultaneous protection against cardiomyocyte apoptosis and necrosis during myocardial ischemia and reperfusion, FASEB J. 15 (2001) 393–402.
[25] R. Barbato, R. Menabo, P. Dainese, E. Carafoli, S. Schiaffino, F. Di Lisa, Binding of cytosolic proteins to myofibrils in ischemic rat hearts, Circ. Res. 78 (1996) 821–828.
[26] N. Golenhofen, A. Arbeiter, R. Koob, D. Drenckhahn, Ischemia-induced association of the stress protein alpha B-crystallin with I-band portion of cardiac titin, J. Mol. Cell Cardiol. 34 (2002) 309–319.
[27] P. Vicart, A. Caron, P. Guicheney, Z. Li, M.C. Prevost, A. Faure, D. Chateau, F. Chapon, F. Tome, J.M. Dupret, D. Paulin, M. Fardeau, A missense mutation in the alphaB-crystallin chaperone gene causes a desmin-related myopathy, Nat. Genet. 20 (1998) 92–95.
[28] D. Selcen, A.G. Engel, Myofibrillar myopathy caused by novel dominant negative alpha B-crystallin mutations, Ann. Neurol. 54 (2003) 804–810.
[29] B. Bullard, C. Ferguson, A. Minajeva, M.C. Leake, M. Gautel, D. Labeit, L. Ding, S. Labeit, J. Horwitz, K.R. Leonard, W.A. Linke, Association of the chaperone alphaB-crystallin with titin in heart muscle, J. Biol. Chem. 279 (2004) 7917–7924.
[30] L. Tskhovrebova, J. Trinick, Titin: properties and family relationships, Nat. Rev. Mol. Cell. Biol. 4 (2003) 679–689.
[31] H.L. Granzier, S. Labeit, The giant protein titin: a major player in myocardial mechanics, signaling, and disease, Circ. Res. 94 (2004) 284–295.
[32] B. Gerull, M. Gramlich, J. Atherton, M. McNabb, K. Trombitas, S. Sasse-Klaassen, J.G. Seidman, C. Seidman, H. Granzier, S. Labeit, M. Frenneaux, L. Thierfelder, Mutations of TTN, encoding the giant muscle filament titin, cause familial dilated cardiomyopathy, Nat. Genet. 30 (2002) 201–204.
[33] T. Hayashi, T. Arimura, M. Itoh-Satoh, K. Ueda, S. Hohda, N. Inagaki, M. Takahashi, H. Hori, M. Yasunami, H. Nishi, Y. Koga, H. Nakamura, M. Matsuzaki, B.Y. Choi, S.W. Bae, C.W. You, K.H. Han, J.E. Park, R. Knoll, M. Hoshijima, K.R. Chien, A. Kimura, Tcap gene mutations in hypertrophic cardiomyopathy and dilated cardiomyopathy, J. Am. Coll. Cardiol. 44 (2004) 2192–2201.
[34] O. Nakagawa, Y. Ogawa, H. Itoh, S. Suga, Y. Komatsu, I. Kishimoto, K. Nishino, T. Yoshimasa, K. Nakao, Rapid transcriptional activation and early mRNA turnover of brain natriuretic peptide in cardiocyte hypertrophy. Evidence for brain natriuretic peptide as an "emergency" cardiac hormone against ventricular overload, J. Clin. Invest. 96 (1995) 1280–1287.
[35] L.E. Morrison, R.J. Whittaker, R.E. Klepper, E.F. Wawrousek, C.C. Glembotski, Roles for alphaB-crystallin and HSPB2 in protecting the myocardium from ischemia-reperfusion-induced damage in a KO mouse model, Am. J. Physiol. Heart Circ. Physiol. 286 (2004) H847–H855.
[36] M.D. Perng, S.F. Wen, I.P. van den, A.R. Prescott, R.A. Quinlan, Desmin aggregate formation by R120G alphaB-crystallin is caused by altered filament interactions and is dependent upon network status in cells, Mol. Biol. Cell 15 (2004) 2335–2346.
[37] T. Hayashi, T. Arimura, K. Ueda, H. Shibata, S. Hohda, M. Takahashi, H. Hori, Y. Koga, N. Oka, T. Imaizumi, M. Yasunami, A. Kimura, Identification and functional analysis of a caveolin-3 mutation associated with familial hypertrophic cardiomyopathy, Biochem. Biophys. Res. Commun. 313 (2004) 178–184.
[38] S. Daehmlow, J. Erdmann, T. Knueppel, C. Gille, C. Froemmel, M. Hummel, R. Hetzer, V. Regitz-Zagrosek, Novel mutations in sarcomeric protein genes in dilated cardiomyopathy, Biochem. Biophys. Res. Commun. 298 (2002) 116–120.
[39] B. Mohapatra, S. Jimenez, J.H. Lin, K.R. Bowles, K.J. Coveler, J.G. Marx, M.A. Chrisco, R.T. Murphy, P.R. Lurie, R.J. Schwartz, P.M. Elliott, M. Vatta, W. McKenna, J.A. Towbin, N.E. Bowles, Mutations in the muscle LIM protein and alpha-actinin-2 genes in dilated cardiomyopathy and endocardial fibroelastosis, Mol. Genet. Metab. 80 (2003) 207–215.
[40] S. Lange, D. Auerbach, P. McLoughlin, E. Perriard, B.W. Schafer, J.C. Perriard, E. Ehler, Subcellular targeting of metabolic enzymes to titin in heart muscle may be mediated by DRAL/FHL-2, J. Cell Sci. 115 (2002) 4925–4936.

nature medicine

ARTICLES

Chondromodulin-I maintains cardiac valvular function by preventing angiogenesis

Masatoyo Yoshioka[1,2], Shinsuke Yuasa[1,2], Keisuke Matsumura[1,2], Kensuke Kimura[1,2], Takayuki Shiomi[3], Naritaka Kimura[1,4], Chisa Shukunami[5], Yasunori Okada[3], Makio Mukai[6], Hankei Shin[4], Ryohei Yozu[4], Masataka Sata[7], Satoshi Ogawa[2], Yuji Hiraki[5] & Keiichi Fukuda[1]

The avascularity of cardiac valves is abrogated in several valvular heart diseases (VHDs). This study investigated the molecular mechanisms underlying valvular avascularity and its correlation with VHD. Chondromodulin-I, an antiangiogenic factor isolated from cartilage, is abundantly expressed in cardiac valves. Gene targeting of chondromodulin-I resulted in enhanced Vegf-A expression, angiogenesis, lipid deposition and calcification in the cardiac valves of aged mice. Echocardiography showed aortic valve thickening, calcification and turbulent flow, indicative of early changes in aortic stenosis. Conditioned medium obtained from cultured valvular interstitial cells strongly inhibited tube formation and mobilization of endothelial cells and induced their apoptosis; these effects were partially inhibited by chondromodulin-I small interfering RNA. In human VHD, including cases associated with infective endocarditis, rheumatic heart disease and atherosclerosis, VEGF-A expression, neovascularization and calcification were observed in areas of chondromodulin-I downregulation. These findings provide evidence that chondromodulin-I has a pivotal role in maintaining valvular normal function by preventing angiogenesis that may lead to VHD.

A balance of angiogenic and antiangiogenic factors is critical to normal development and organ homeostasis. Although the heart is a vascular-rich organ, cardiac valves are avascular and oxygen supply is via diffusion from the blood stream[1]. Under pathological conditions such as atherosclerosis, rheumatic valvular heart disease (RHD) or infective endocarditis, cardiac valves express angiogenic factors leading to neovascularization[2,3]. The contribution of antiangiogenic factors to the maintenance of avascularity in cardiac valves is unknown.

The mesenchymal cells of cardiac valve tissue, known as valvular interstitial cells (VICs), have an incomplete basal lamina, are sparsely distributed, and have direct and extensive contacts with collagen fibers, elastin microfibrils and proteoglycans of the extracellular matrix[4–6]. Cartilage is another avascular tissue, and transcription factors considered essential for chondrogenesis during endochondral ossification, including Sox9 (ref. 7), NFATc[8], Cbfa1 (ref. 9) and MSX2 (ref. 10), and growth factors such as BMP2 (ref. 11) and TGFß2 (ref. 12), are also expressed in developing cardiac valves. Sox9, in conjunction with Sox5 and Sox6, can induce the expression of genes specific to cartilage, including chondromodulin-1 (encoded by *Chm1*, also known as *Lect1*), even in nonchondrogenic cells[13], and are essential to cardiac valve development[7]. Chm-I is a 121–amino acid residue glycoprotein derived from a 335–amino acid residue type II transmembrane precursor located primarily in avascular tissue of the eye and cartilage[14,15]. After translation, the Chm-I precursor is cleaved by furin proteases[16], and secreted Chm-I accumulates in the interstitial space of the cartilage matrix[17]. The inhibition of endothelial cell proliferation and tube morphogenesis by Chm-I provided the first evidence of the antiangiogenic activity of this protein[17–20].

The aim of this study was to determine the role of antiangiogenic factors in valvular heart disease (VHD). We show that CHM-I is expressed strongly in normal cardiac valves, but at markedly reduced levels in human VHD and *Apoe*$^{-/-}$ mice. We also provide direct evidence that Chm-I has a role as an antiangiogenic factor by showing that loss of Chm-I leads to neovascularization, as well as unusual calcification and infiltration of inflammatory cells into the matrix of cardiac valves. These data provide new insight into the mechanisms underlying maintenance of avascularity in cardiac valves and the disruption of this process in pathological conditions. Understanding these mechanisms may form the basis of new therapeutic regimens for the treatment of VHD.

RESULTS

Cardiac valves express chondromodulin-I

RT-PCR for *Chm1* showed a faint level of expression in the heart, cartilage and eye (**Supplementary Fig. 1** online). *Chm1* expression was strong in cardiac valves, but absent from the atrium and ventricle. Expression of *Chm1* first appeared in the heart at embryonic day (E) 9.5 and persisted in the adult. Quantitative PCR showed that *Chm1*

[1]Department of Regenerative Medicine and Advanced Cardiac Therapeutics; [2]Cardiopulmonary Division, Department of Internal Medicine; [3]Department of Pathology; [4]Department of Cardiovascular Surgery; Keio University School of Medicine, 35 Shinanomachi, Shinjuku-ku, Tokyo 160-8582, Japan. [5]Department of Cellular Differentiation, Institute for Frontier Medical Sciences, Kyoto University, 53 Shogoin-Kawahara-cho, Sakyo-ku, Kyoto 606-8507, Japan. [6]Division of Diagnostic Pathology, Keio University School of Medicine, 35 Shinanomachi, Shinjuku-ku, Tokyo 160-8582, Japan. [7]Department of Cardiovascular Medicine, University of Tokyo Graduate School of Medicine, 7-3-1 Hongo, Bunkyo-ku, Tokyo 113-8655, Japan. Correspondence should be addressed to K.F. (kfukuda@sc.itc.keio.ac.jp).

Received 29 November 2005; accepted 22 August 2006; published online 17 September 2006; doi:10.1038/nm1476

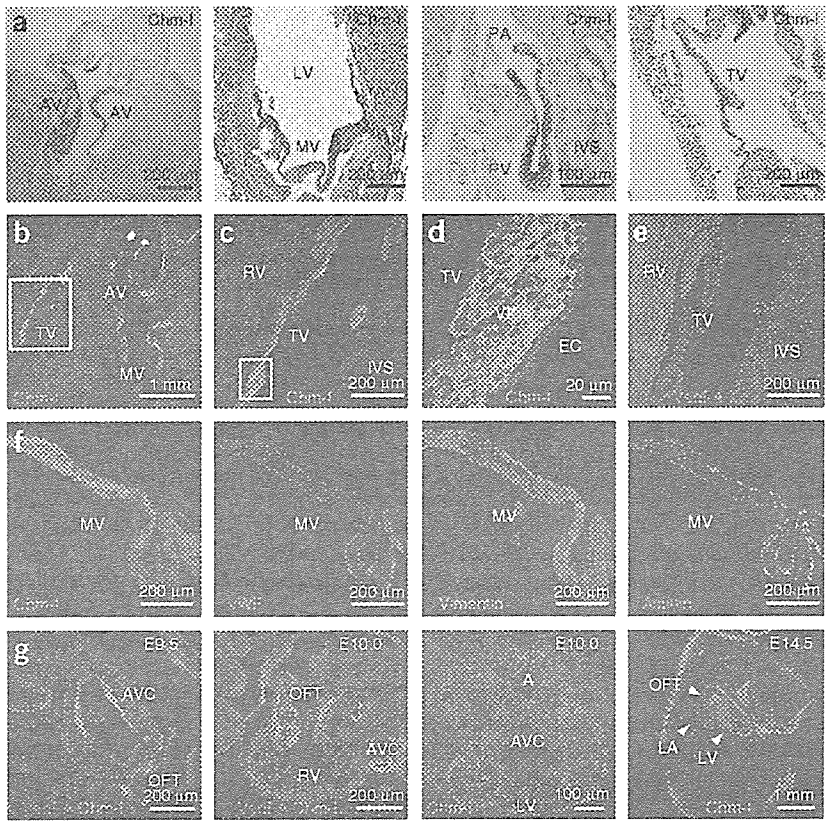

Figure 1 Immunohistochemistry and immunofluorescence staining of Chm-I protein in developing and adult mouse heart. (**a**) Chm-I was expressed in all four valves in the adult. Positive signals are shown in brown. The left two micrographs are views along the short axis; the right two micrographs are views along the long axis. AV, aortic valve; IVS, interventricular septum; LV, left ventricle; MV, mitral valve; PA, pulmonary artery; PV, pulmonary valve. (**b**–**e**) Immunofluorescence staining for Chm-I and Vegf-A in the adult mouse heart. The boxed region in **b** is shown in **c** and **e**; the boxed region in **c** is shown in **d**. (**f**) Serial sections of the mitral valve immunostained for Chm-I, vWF, vimentin and actinin. (**g**) Immunofluorescence staining for Chm-I and Vegf-A in various developmental stages. A, atrium; AVC, atrioventricular cushion; EC, endothelial cell; LA, left atrium; OFT, outflow tract; RV, right ventricle; TV, tricuspid valve.

expression was 800 times higher in cardiac valves than in the atrium or ventricle. Western-blot analysis identified the 25-kDa mature glycosylated form of Chm-I in rat and human cardiac valves, which was also present in cartilage.

Immunohistochemical analysis

Immunohistochemistry (**Fig. 1** and **Supplementary Fig. 2** online) showed localization of Chm-I to all four cardiac valves. Analysis of serial sections showed that Chm-I and Vegf-A expression did not overlap. Chm-I was detected throughout the VICs and extracellular matrix, but not in the outer endothelial cell layer.

During development, cardiac valve precursor cells from the atrioventricular cushions and outflow tract express Chm-I from E9.5. In E10.0 embryos, Chm-I is expressed in the cardiac jelly covering the trabeculating cardiomyocytes of the left ventricle, the outer curvature of the right ventricle and the outflow tract. Chm-I expression in the ventricles decreased gradually as development progressed, and by mid-embryogenesis, both transcripts and protein were absent. The non-overlapping localization of Chm-I and Vegf-A was apparent at all development stages.

Chm1 disruption induces angiogenesis in cardiac valves

Cardiac valves of 8-week-old $Chm1^{-/-}$ mice were histologically similar to those of wild-type mice. By old age (90.2 ± 7.4 weeks), the aortic valves of $Chm1^{-/-}$ mice were significantly more bulky and the density of VICs more sparse than in age-matched wild-type mice ($P < 0.05$; **Fig. 2**). The mean thickness of the aortic valve gradually increased after 32 weeks and reached a thickness 1.8 times greater than that of wild-type mice at 90 weeks. No significant morphological changes were observed in the mitral or other valves ($P < 0.05$ at 90 weeks). Cardiac valves of $Chm1^{-/-}$ mice had newly developed capillary-like structures and were Chm-I–negative and Vegf-A–positive. Vegf-A expression was not observed in valves from young adults but was upregulated in aged animals. Cells forming capillary-like structures were positive for von Willebrand factor (vWF)–specific antibody, confirming that they were endothelial cells. Calcium deposits in the cardiac valves of $Chm1^{-/-}$ mice were detected with von Kossa staining, and the presence of inflammatory cells was confirmed by Mac-1 staining. New vessel formation and invasion of inflammatory cells are indicative of sclerotic processes. Sudan IV staining showed that affected valves were laden with lipid. Deposits of calcium and lipid were relatively large at the laminae ventricularis compared with the other laminae. $Chm1^{+/+}$ littermates did not show these characteristics. Capillary structures in three leaflets of the aortic valve were counted in each 20-μm section. The capillary number in $Chm1^{-/-}$ mice was 13.8 times higher than that in $Chm1^{+/+}$ mice ($P < 0.01$). The aortic valves showed strong expression of Vegf-A, enhanced *de novo* capillary-like structures, increased calcium and lipid deposits, and Mac-1–positive staining. Changes in these characteristics were not notable in other valves.

Early phase aortic stenosis in $Chm1^{-/-}$ mice

Echocardiography revealed bright echogenic aortic valves that moved backward and forward with slight acoustic shadowing, suggestive of thickening or calcification (**Fig. 3**). A color Doppler study showed a mosaic turbulent jet distal to the aortic valve. No echogenic object or turbulent jet was observed in $Chm1^{+/+}$ mice. An M-mode scan showed marked thickening of the aortic valve. There were no significant differences between $Chm1^{+/+}$ and $Chm1^{-/-}$ mice in left ventricular wall thickness, left ventricular end-diastolic and end-systolic dimensions, ejection fraction, brightness of the mitral valve, or turbulent flow in the area of the mitral valve. The area trace of the aortic valve gradually increased from 32 weeks ($P < 0.01$) and had increased approximately 3.8-fold by 90 weeks ($P < 0.001$).

Analysis of sclerotic cardiac valves in $Apoe^{-/-}$ mice

The expression of antiangiogenic Chm-I and angiogenic Vegf-A was examined in the cardiac valves of aged $Apoe^{-/-}$ mice (87.3 ± 5.3 weeks

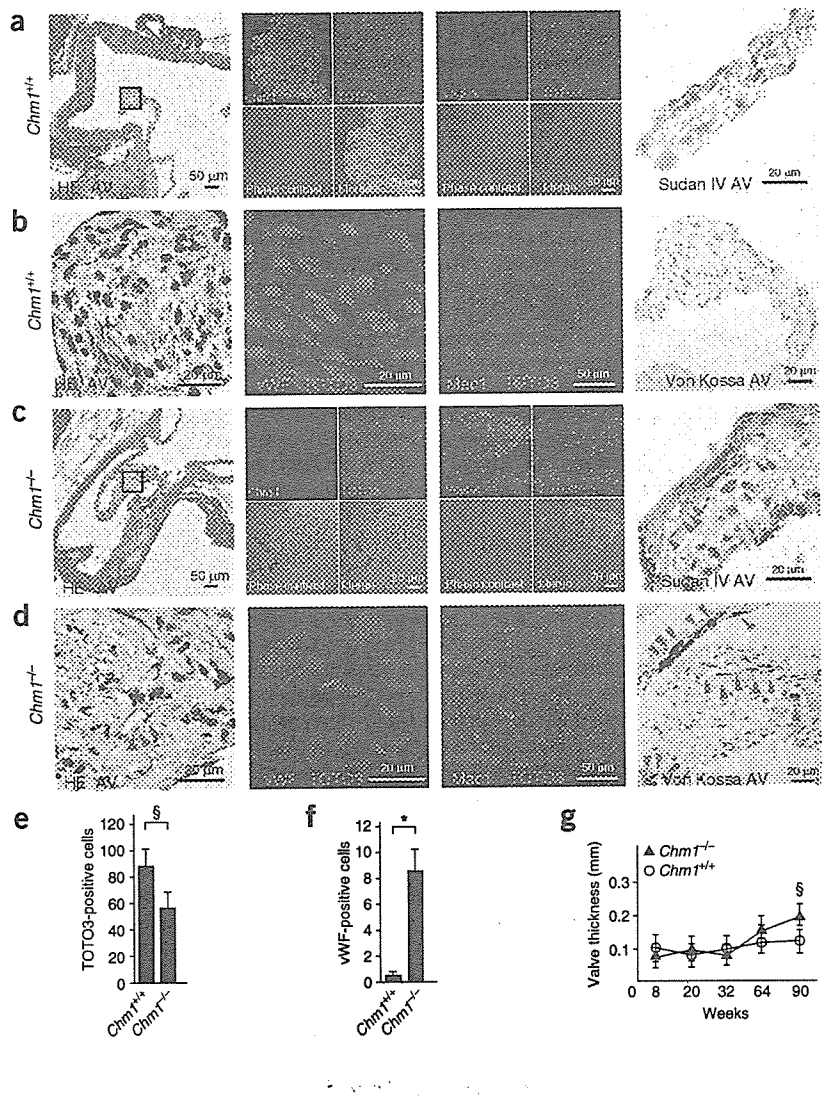

Figure 2 Abnormal angiogenesis, inflammatory cell infiltration and mineralization in cardiac valves of aged *Chm1*$^{-/-}$ mice. (**a**,**c**) Hematoxylin and eosin staining of aortic valves in aged *Chm1*$^{-/-}$ and age-matched wild-type mice at low magnification. *Chm1*$^{-/-}$ mice had bulky leaflets. *Chm1*$^{-/-}$ mice were confirmed negative for Chm-I immunostaining. Vegf-A staining in the aortic valve showed a strong positive signal only in *Chm1*$^{-/-}$ mice. Only *Chm1*$^{-/-}$ mice exhibited lipid deposits (arrowheads) by Sudan IV staining. (**b**,**d**) Hematoxylin and eosin staining at high magnification. Capillary-like structures (arrowheads) were observed only in aged *Chm1*$^{-/-}$ mice. The cell density decreased at the neovascular area. Immunofluorescence staining for vWF and Mac-1 are shown; positive signals were observed only in *Chm1*$^{-/-}$mice. Von Kossa staining showed calcium deposits in *Chm1*$^{-/-}$ mice (arrowheads). The boxed regions in **a** and **c** are shown in **b** and **d**, respectively. The cell density (**e**) and the number of vWF-positive cells (**f**) in three leaflets of the aortic valve were counted for every 20-μm section stained for immunofluorescence in which at least one leaflet was visible. The cell density and the number of vWF-positive cells were determined at 90 weeks of age for *Chm1*$^{-/-}$ ($n = 12$) and *Chm1*$^{+/+}$ ($n = 12$) mice. (**g**) The mean thickness of the aortic valves was investigated at 8, 20, 32, 64 and 90 weeks of age. §$P < 0.05$; *$P < 0.01$.

old, $n = 10$) as a model of atherosclerosis with abnormal lipid deposits and calcification in cardiac valves. Chm-I was absent from calcified regions (**Fig. 4**) in aortic and mitral valves containing Vegf-A positive cells. Age-matched wild-type mice (88.5 ± 4.8 weeks old, $n = 8$) showed the expected physiological Chm-I–positive and Vegf-A–negative expression pattern and no sclerotic changes or calcification. *In situ* hybridization for *Chm1* showed no signal in the sclerotic aortic valve leaflet in *Apoe*$^{-/-}$ mice, whereas age-matched wild-type mice showed positive signals. The Chm-I–positive area in aged *Apoe*$^{-/-}$ mice was less than 48.0% the size of that in age-matched wild-type mice ($P < 0.01$). The Vegf-A–positive area and the microvessel density in aged *Apoe*$^{-/-}$ mice were significantly greater compared with age-matched wild-type mice ($P < 0.01$).

VIC-derived Chm-I directly suppresses angiogenesis

We next investigated whether VICs produce Chm-I and, if so, whether VIC-derived Chm-I can affect proliferation or tube morphogenesis of human coronary artery endothelial cells (HCAECs). Primary VICs were obtained from explant cultures of rat cardiac valves (**Fig. 5**). Explanted cells comprise a heterogeneous population of cobblestone and spindle-type cells characteristic of VICs after 3 d (ref. 21) and formed an orthogonal pattern of overgrowth[5]. The cells were negative for the acetyl-LDL–DiI conjugate, consistent with cardiac valves being composed of VICs. Immunostaining showed Chm-I in the cytoplasm of VICs and the absence of Chm-I in NIH3T3 cells. RT-PCR and western-blot analysis confirmed that VICs secreted Chm-I into the culture media. Furthermore, Chm-I secretion was inhibited by treatment of VICs with specific small interfering RNA (siRNA).

HCAECs formed capillary-like tube structures on Matrigel after 6 h (ref. 22). Capillary-like structures were less prominent following treatment with conditioned medium from VICs (VIC-CM) compared with mock medium or conditioned medium from control NIH3T3 cells (NIH3T3-CM). HCAECs cultured with conditioned medium from siRNA-treated VICs regained their ability to form capillary-like structures. The total length of capillary-like structures was evaluated using NIH image software. Quantitative analysis of the length of tube formation compared with controls showed that VIC-CM inhibited tube formation by 75.9% ($P < 0.001$) and that *Chm1*-specific siRNA led to recovery of tube formation capacity by 62.9% ($P < 0.001$).

Chm-I also inhibited the migration capacity of HCAECs. In a modified Boyden chamber assay, HCAECs cocultured with VICs lost their migratory capacity compared with NIH3T3 cells. Treatment of VICs with *Chm1*-specific siRNA led to HCAECs partially regaining migratory capacity. Control siRNA had no effect on VIC-mediated inhibition of migration. Quantitative analysis showed that VICs decreased the number of migrated cells by 82.1% ($P < 0.001$), and that siRNA specific to *Chm1* recovered the migratory capacity by 25.7% ($P < 0.01$). These results imply that Chm-I has a pivotal role as a chemoattractant-inhibitor in cardiac valves.

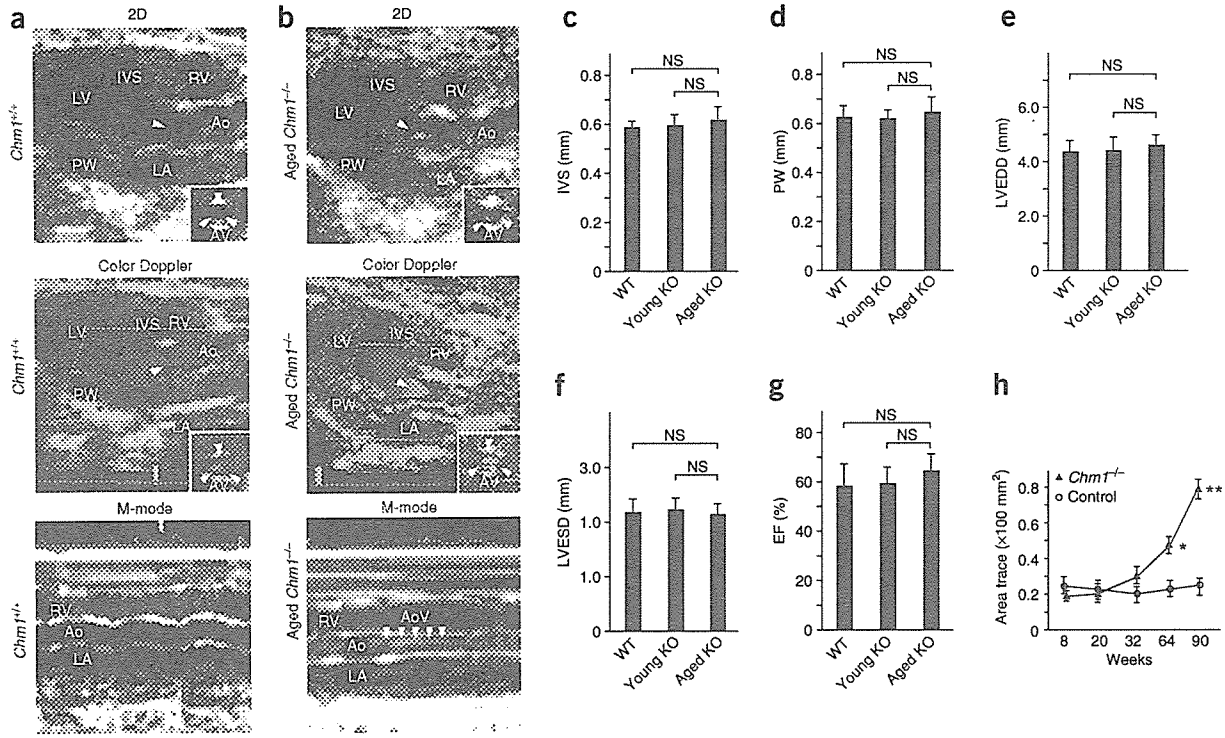

Figure 3 Echocardiography of *Chm1*$^{-/-}$ mouse hearts. **(a,b)** Top, two-dimensional echocardiography showed an abnormal bright echogenic mass in the aortic valve leaflets in *Chm1*$^{-/-}$ mice that were not detected in the aortic valves of *Chm1*$^{+/+}$ mice. Middle, a color Doppler study showed a mosaic turbulent jet distal to the aortic valve in *Chm1*$^{-/-}$ mice that was not detected in the aortic valve of *Chm1*$^{+/+}$ mouse hearts. Inset shows the aortic valve level short-axis view of each long-axis figure. Bottom, M-mode scanning of the aortic valve area. Arrowheads indicate the thickened and calcified aortic valve leaflets in *Chm1*$^{-/-}$ mice. Mice were 90 weeks of age. **(c)** Thickness of the interventricular septum. **(d)** Thickness of the left ventricular posterior wall. **(e)** Left ventricular end-diastolic dimension (LVEDD). **(f)** Left ventricular end-systolic dimension (LVESD). **(g)** Ejection fraction (EF). **(h)** Time course of the area trace of the aortic valve. WT, wild-type; young KO, young adult knockout mice at 8 and 20 weeks of age; aged KO, young adult knockout mice at 90 weeks of age; Ao, aorta; AV, aortic valve; IVS, interventricular septum; LA, left atrium; LV, left ventricle; LVFW, left ventricular free wall; PW, posterior wall; RV, right ventricle. §$P < 0.05$; *$P < 0.01$; NS, not significant.

Morphological changes in HCAECs following treatment with VIC-CM were suggestive of apoptosis. To determine whether Chm-I induces apoptosis, we stained HCAECs treated with VIC-CM with Annexin V and propidium iodide. Positive staining for Annexin V–fluorescein isothiocyanate (FITC) showed induction of apoptosis, and fluorescent cells were both propidium iodide–positive (early apoptotic labeling pattern) and –negative (late apoptotic labeling pattern). HCAECs treated with NIH3T3-CM were Annexin V–FITC–negative. Annexin V–FITC–positive fluorescent cells increased by 8.0-fold in VIC-CM–treated cells ($P < 0.01$). VIC-CM treated with siRNA specific to *Chm1* strongly attenuated VIC-mediated apoptosis ($P < 0.01$). The antiangiogenic activity of Chm-I was confirmed by examining the effects of purified recombinant human CHM-I on tube formation and migration *in vitro*. The recombinant human CHM-I inhibited tube formation and migration in HCAECs and induced apoptosis in a dose-dependent manner (**Supplementary Fig. 3** online). To test whether Chm-I has hyperplastic or cell survival effects on VICs, cell survival was assessed using the MTT assay with or without siRNA specific to *Chm1*. We found no significant difference in survival between VICs treated with siRNA specific to *Chm1* and untreated VICs or VICs treated with control siRNA. This result indicates that Chm-I is not a survival factor for VICs (**Supplementary Fig. 4** online). These findings imply that Chm-I protects cardiac valves from endothelial infiltration and vascular formation.

Pathological analysis of human cardiac valves

Hematoxylin and eosin staining and immunostaining of autopsy or surgical specimens were used to determine the expression profile of CHM-I and VEGF-A in cardiac valves of patients with VHD (**Fig. 6**). Blood vessels were absent from cardiac valves of patients without VHD. In normal valves, CHM-I was detected in the laminae fibrosa, spongiosa and ventricularis layers, but not in endothelial cells, whereas VEGF-A was absent from all cell layers. By comparison, numerous vessels were observed in cardiac valves of patients with atherosclerosis, RHD and infective endocarditis. CHM-I was markedly downregulated in regions of new vessel formation that strongly expressed VEGF-A. In normal cardiac valves, or areas without neovascular formation in infective endocarditis and RHD valves, cells stained with vimentin and the interstitial space stained strongly with CHM-I. This result suggests the cells were VICs. By comparison, in regions of neovascularization in diseased valves, the vWF-positive cells adjacent to newly developed vessels were endothelial cells and were at a higher cell density than in normal cardiac valves. Coimmunostaining showed localization of CBFA-1 to the neovascular area of diseased valves in which CHM-I was downregulated, but the absence of CBFA-1 in normal cardiac valves or regions of diseased valves lacking neovascularization (**Supplementary Fig. 5** online).

Matrix metalloproteinases (MMPs) are important in repair and remodeling of damaged tissue, and in early atherosclerosis. We thus

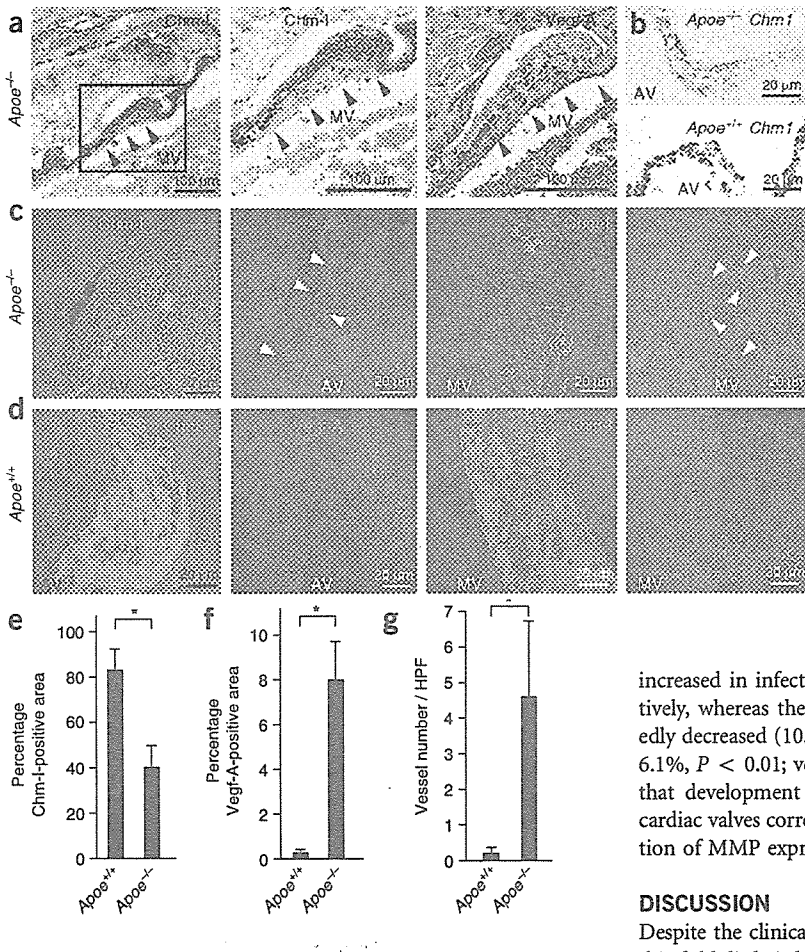

Figure 4 Immunohistochemistry, immunofluorescence staining and *in situ* hybridization of Chm-I and Vegf-A in sclerotic lesions of aged *Apoe*$^{-/-}$mouse hearts. (**a**) Left, immunohistochemistry of Chm-I and Vegf-A in a sclerotic lesion (arrowheads) of the mitral valve (MV) of an *Apoe*$^{-/-}$ mouse heart. Boxed area is enlarged in the middle panel. Right, an adjacent section was immunostained using the Vegf-A–specific antibody. (**b**) *In situ* hybridization of *Chm1* in *Apoe*$^{-/-}$ and age-matched *Apoe*$^{+/+}$ mouse aortic valves (AV). (**c**,**d**) Immunofluorescence staining of Chm-I and Vegf-A in *Apoe*$^{-/-}$ (**c**) and age-matched *Apoe*$^{+/+}$ mice (**d**). Vegf-A was markedly upregulated in the sclerotic valve area where Chm-I was downregulated in *Apoe*$^{-/-}$ mice. Arrowheads indicate the valvular area in which Chm-I was downregulated and Vegf-A was upregulated in *Apoe*$^{-/-}$ mice. (**e**,**f**) Quantitative analysis of the percentage of the Chm-I–positive area and the Vegf-A–positive area in the cardiac valves of *Apoe*$^{+/+}$ and *Apoe*$^{-/-}$ mice. (**g**) Quantitative analysis of the microvessel density in the cardiac valves of *Apoe*$^{+/+}$ and *Apoe*$^{-/-}$ mice. $^{*}P < 0.01$.

investigated the colocalization of MMPs and CHM-I in various VHDs (**Supplementary Fig. 6** online). In the atherosclerotic valve, MMP-1, MMP-2, MMP-9 and MMP-13 showed positive signals, whereas in the infective endocarditis and RHD valves, only MMP-1, MMP-2 and MMP-13 showed positive signals. By comparison, MMP-1 and MMP-2 showed weak signals in valves with annuloaortic ectasia and no signal in the individuals without VHD. Furthermore, expression of MMPs and CHM-I was mutually exclusive. The cells in the MMP-positive area stained positive for vimentin, desmin (data not shown), and α-smooth muscle actin (**Supplementary Fig. 7** online). In the atherosclerotic valve, but not in infective endocarditis and RHD valves, some cells were positive for CD11b and CD14 (data not shown). MMP expression in atherosclerotic valves was different from that in valves from patients without VHD, and the interstitial space did not stain positive for CHM-I as in normal valves. These results suggest that the cells staining positive for CD11b and CD14 are not VICs but infiltrating macrophages or activated myofibroblasts. This pathological expression profile was not observed in the cardiac valves of patients with annuloaortic ectasia or rupture of the chordae tendineae of the mitral valve. Computer image analysis showed that vessel number (7.7 ± 1.8, $P < 0.01$; 7.1 ± 1.3, $P < 0.01$; 6.0 ± 1.9, $P < 0.01$; versus 0 ± 0 in control), calcification area (1.6 ± 0.6%, $P < 0.05$; 4.1 ± 0.7%, $P < 0.01$; 5.0 ± 0.5%, $P < 0.01$; versus 0 ± 0% in control), and the percentage of VEGF-A–positive cells (22.9 ± 6.0%, $P < 0.01$; 31.1 ± 9.4%, $P < 0.01$; 18.5 ± 6.2%, $P < 0.01$; versus 1.5 ± 0.3% in control) were markedly increased in infective endocarditis, RHD and atherosclerosis, respectively, whereas the percentages of CHM-I–positive cells were markedly decreased (10.0 ± 3.2%, $P < 0.01$; 4.9 ± 2.2%, $P < 0.01$; 25.8 ± 6.1%, $P < 0.01$; versus 72.2 ± 6.1% in control). These findings show that development of angiogenesis and sclerotic change in diseased cardiac valves correlate with downregulation of CHM-I and upregulation of MMP expression levels.

DISCUSSION

Despite the clinical importance of heart disease and intense study in this field, little is known of the mechanisms underlying the degeneration of cardiac valves. The present study addresses this issue by demonstrating the key role of the potent antiangiogenic factor Chm-I in the prevention of VHD by maintaining the avascular nature of cardiac valves.

Chm-I is expressed in the cartilage, eye and thymus of various species including human[23], rabbit[19], mouse[24], chick[25,26], cow[14] and zebra fish[27]. The present study showed that Chm-I expression persisted in normal cardiac valves throughout life but was downregulated in diseased cardiac valves, suggesting that Chm-I has an important role in maintenance of cardiac valve function. The conceptual framework for this role of Chm-I is shown in **Supplementary Figure 8** online. Expression of endostatin, an antiangiogenic factor, is enhanced in aortic valves under pathological, but not normal conditions[28]. The present study is the first report, to our knowledge, of an antiangiogenic factor expressed in cardiac valves under physiological conditions to suppress neovascularization. As cardiac valves are flow-regulating tissues in a dynamic chambered pump, they are subjected to mechanical stress and damage of the endothelial cell lining on the outer layer of the valve. Chm-I may protect cardiac valves from inflammation and vascularization resulting from mechanical damage. To confirm this hypothesis, we analyzed Chm-I expression profiles in cardiac valves in normal and diseased states, in various *in vitro* functional assays, in *Chm1*$^{-/-}$ mice and in *Apoe*$^{-/-}$ mice as an *in vivo* model of cardiac valve disease. The mutually exclusive expression pattern of Chm-I and Vegf-A can be explained by several mechanisms. First, an upstream signal may control the genetic switch between angiogenic and

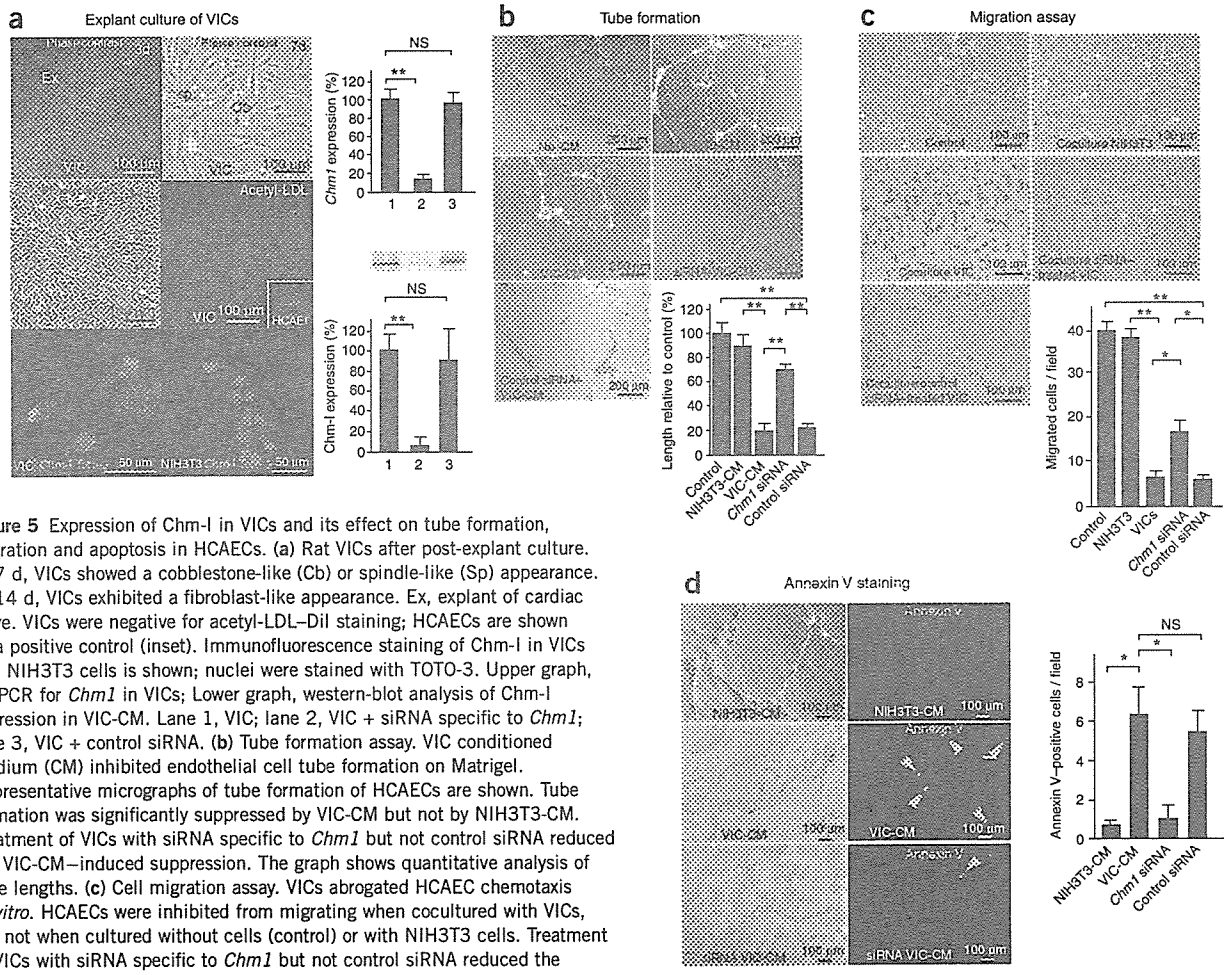

Figure 5 Expression of Chm-I in VICs and its effect on tube formation, migration and apoptosis in HCAECs. (a) Rat VICs after post-explant culture. At 7 d, VICs showed a cobblestone-like (Cb) or spindle-like (Sp) appearance. At 14 d, VICs exhibited a fibroblast-like appearance. Ex, explant of cardiac valve. VICs were negative for acetyl-LDL–DiI staining; HCAECs are shown as a positive control (inset). Immunofluorescence staining of Chm-I in VICs and NIH3T3 cells is shown; nuclei were stained with TOTO-3. Upper graph, RT-PCR for *Chm1* in VICs; Lower graph, western-blot analysis of Chm-I expression in VIC-CM. Lane 1, VIC; lane 2, VIC + siRNA specific to *Chm1*; lane 3, VIC + control siRNA. (b) Tube formation assay. VIC conditioned medium (CM) inhibited endothelial cell tube formation on Matrigel. Representative micrographs of tube formation of HCAECs are shown. Tube formation was significantly suppressed by VIC-CM but not by NIH3T3-CM. Treatment of VICs with siRNA specific to *Chm1* but not control siRNA reduced the VIC-CM–induced suppression. The graph shows quantitative analysis of tube lengths. (c) Cell migration assay. VICs abrogated HCAEC chemotaxis *in vitro*. HCAECs were inhibited from migrating when cocultured with VICs, but not when cultured without cells (control) or with NIH3T3 cells. Treatment of VICs with siRNA specific to *Chm1* but not control siRNA reduced the suppression of chemotaxis. The graph shows quantitative analysis of cell migration. (d) Induction of apoptosis by VIC-CM. HCAECs cultured with NIH3T3-CM (negative control, upper panels) or VIC-CM (middle panels) were treated with FITC-conjugated Annexin V. Treatment of VICs with siRNA specific to *Chm1* reduced the number of Annexin V–positive cells (lower panels). Arrowheads show Annexin V–positive cells. The graph shows quantitative analysis of Annexin V staining. $*P < 0.01$; $**P < 0.001$; NS, not significant.

antiangiogenic factors. In support of this mechanism, genetic rescue in Cbfa1-knockout mice showed that Cbfa1, a critical transcription factor mediating endochondral ossification in cartilage, induced a coordinated change in upregulation of Vegf-A and downregulation of Chm-I in chondrocytes[29]. Cbfa1 expression was shown to be upregulated in atherosclerotic aortic valves[9]. It is possible that upregulated Cbfa1 represses Chm-I and activates Vegf-A. Second, it is possible that loss of VICs may be induced by acute inflammation of cardiac valves in RHD or infective endocarditis; excessive mechanical stress imposed on valves, such as the bicuspid aortic valves; hypertension; or the chronic inflammation found in atherosclerosis. A decrease in VIC number may lead to a reduction in the level of Chm-I produced by diseased valves, and then to the infiltration of Vegf-A–expressing cells. It is also possible that a combination of the above two mechanisms may explain the downregulation of Chm-I and the upregulation of Vegf-A.

Suppression of the antiangiogenic activity of VIC-CM by *Chm1*-specific siRNA suggests that Chm-I is a critical antiangiogenic factor in cardiac valves. The incomplete suppression of antiangiogenic activity implies that VICs may secrete other antiangiogenic factors, similar to those identified in the eye. In the eye, the antiangiogenic factors endostatin and pigment epithelium–derived factor are expressed in addition to Chm-I[30].

The echocardiographic findings of early changes in aortic stenosis, neoangiogenesis, infiltration of inflammatory cells, lipid deposition and calcification were observed only in the cardiac valves of aged *Chm1*$^{-/-}$ mice. The expression of other antiangiogenic factors may delay development of cardiac valve defects such that the phenotype is not apparent during embryogenesis or in the young adult. It is likely that deformation of cardiac valves in aged *Chm1*$^{-/-}$ mice results from ordinary mechanical stress in the absence of the protective antiangiogenic activity of Chm-I. The aortic valve receives the greatest mechanical stress of the four heart valves, which may explain the pathological changes observed in *Chm1*$^{-/-}$ mice. The molecular mechanism underlying the influence of mechanical stress on intracellular signaling needs further investigation.

Previous investigations showed that (i) the expression of angiogenic factors and neoangiogenesis occurs in VHD[2,30–33]; (ii) atherosclerotic plaque progression is associated with angiogenesis[34,35]; (iii) the early lesion of degenerative VHD is an active inflammatory process with

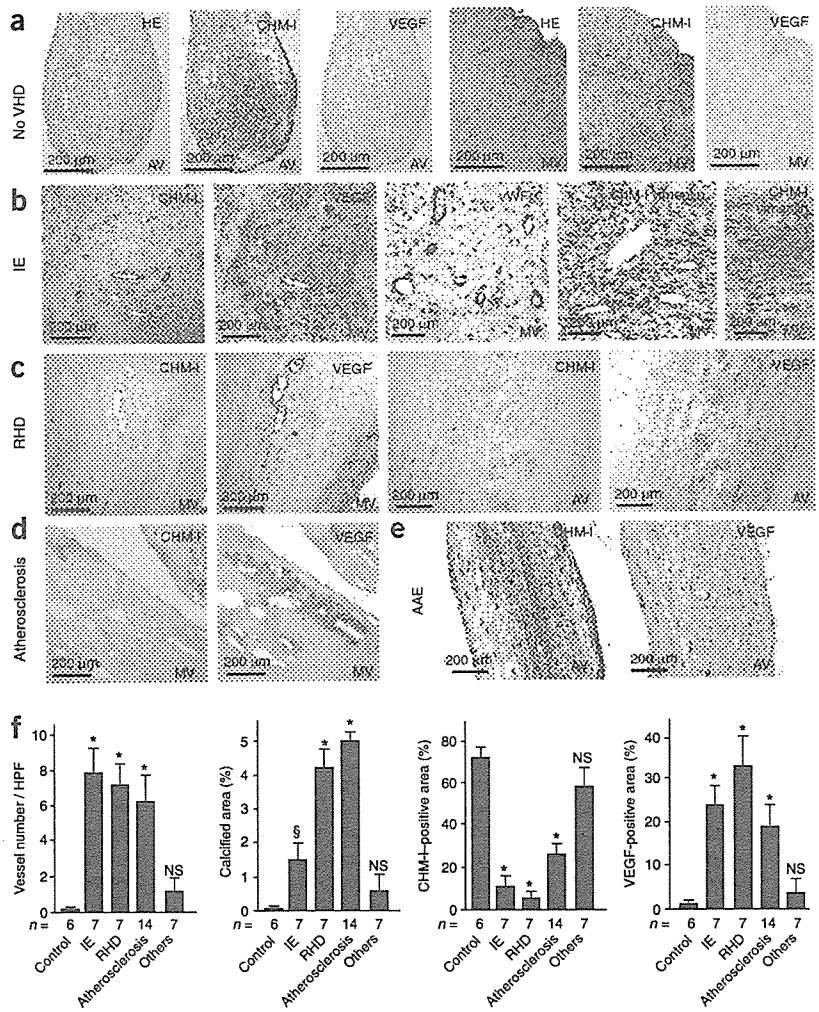

Figure 6 Histology and immunohistochemistry of cardiac valves from human autopsies and surgical samples. (**a**) Samples from autopsies with no VHD. HE, hematoxylin and eosin staining. CHM-I was strongly expressed, whereas VEGF-A was not expressed. (**b–d**) Representative micrographs of immunohistochemistry for surgical samples of various VHDs. Prominent angiogenesis was found in infective endocardit is (IE, **b**), RHD (**c**) and atherosclerotic VHD (**d**). (**e**) The aortic valve in annuloaortic ectasia (AAE) showed no angiogenesis and stained well for CHM-I, but not VEGF-A. In **b**, double immunostaining for CHM-I (brown) and vimentin (purple) is shown in the neovascular and non-neovascular areas in the fourth and fifth micrographs from the left, respectively. The level of CHM-I was markedly diminished in the large area with strong VEGF-A expression and new vessel formation. AV, aortic valve; MV, mitral valve. (**f**) Computer-assisted quantitative analysis of vessel number, calcification area, percentage CHM-I–positive area, and percentage VEGF-A–positive area. $*P < 0.01$; $§P < 0.05$. NS, not significant.

similarities to atherosclerosis[32,36–40]; and (iv) endothelial cells in VHD have significantly increased angiogenic potency[28]. These findings suggest that angiogenesis of cardiac valves results in the progression of sclerogenic change. Further supporting this, it was reported that although VICs in normal valves stained positively for vimentin but not alpha-actin or desmin, VICs in myxomatous valves contained both vimentin and alpha-actin or desmin (characteristics of myofibroblasts) and strongly expressed SMemb, MMPs, cathepsins and IL-1β, which stained weakly in controls. It was concluded that VICs in myxomatous valves have features of activated myofibroblasts and express excessive levels of catabolic enzymes[41]. After an investigation of the expression of MMPs and tissue inhibitor of metalloproteases (TIMPs) in aortic valve disease, it was reported that levels of MMP-3, MMP-9 and TIMP-1 were increased in aortic stenosis[42]. Taken together, the present findings and previous investigations support the hypothesis that antiangiogenic factors protect cardiac valves from angiogenesis and the development of dystrophic changes. By comparison, angiogenic factors and MMPs promote dystrophic changes. Further studies to support this hypothesis include investigations to determine the protective effect of *Chm1* overexpression. The present findings support preclinical investigations of Chm-I, or proteins with a similar function, as therapeutic agents in preventing VHD.

METHODS

RT-PCR. Total RNA was isolated using Trizol reagent (Gibco-BRL) and treated with DNase I (Roche). RT-PCR was carried out as described previously[43] using the following primers: *Chm1*, 5′-CTTAAGCCCATGTATCCAAA-3′ (forward), 3′-CCAGTGGTTCACAGATCTTC-5′ (reverse); *Gapdh*, 5′-TTCAACGGCA CAGTCAAGG-3′ (forward), 3′-CATGGACTGTGGTCATGAG-5′ (reverse).

***In situ* hybridization.** Paraffin-embedded sections were treated with proteinase K, and *in situ* hybridization was carried out as described previously[43]. Template DNA was an 879-bp cDNA encoding mouse *Chm1* cloned into the pCR II-TOPO vector. Color was developed with 0.2 mg ml^{-1} of 3,3′-diaminobenzidine tetrahydrochloride in 50 mmol $liter^{-1}$ Tris HCl, pH 7.6, containing 0.003% hydrogen peroxide. The sections were counterstained with hematoxylin and eosin and were observed under microscopy.

Immunohistochemical and immunofluorescence staining. Adult mouse hearts were perfused from the apex with phosphate-buffered saline, perfusion-fixed with 4% paraformaldehyde in phosphate-buffered saline and used for immunostaining as described previously[15]. The hearts were dissected, immersion-fixed overnight at 4 °C in 4% paraformaldehyde and then embedded in paraffin. Before application of the primary antibodies, paraffin was removed from the sections in xylene and the sections were heated in a microwave oven in 10 mmol citric acid monohydrate (DAKO), pH 6.0, for 3 min. After sections were rinsed in phosphate-buffered saline, they were incubated overnight at 4 °C with 5% normal rabbit serum and affinity-purified rabbit polyclonal antibody to Chm-I, rabbit polyclonal antibody to Vegf-A (1:200 dilution; Santa Cruz Biotechnology), vWF (1:200 dilution; Lab vision Corporation), Mac-1 (1:200 dilution; BD PharMingen, Inc.), Cbfa1 (1:50 dilution; R&D systems), MMP-1 (ref. 44; Daiichi fine chemical), MMP-2 (ref. 44; Daiichi fine chemical), MMP-3 (ref. 44; Daiichi fine chemical), MMP-9 (ref. 44; Daiichi fine chemical), MMP-13 (ref. 44; 1:100 dilution; Biogenesis), α smooth muscle actin (1:400 dilution; Sigma) or CD11b (1:200 dilution; BD PharMingen). Immunohistochemical signals were detected by applying 0.05% 3,3′-diaminobenzidine tetrahydrochloride (Sigma-Aldrich)